Structural determinants of the inhibition of M2R by Sigma-1R and the direct inhibition of GIRK channels by Sigma-1R antagonist

Liu, Chang

The Graduate University for Advanced Studies, SOKENDAI
School of Life Science
Department of Physiological Sciences
2023

Contents

Abbreviations

ALS	Amyotrophic lateral sclerosis
BD1047	BD1047 dihydrobromide
BiP	Immunoglobulin binding protein
CTD	Cytoplasmic tail domain
C-ter	C-terminal
D1R	Dopamine D1 receptor
D2R	Dopamine D2 receptor
ER	Endoplasmic reticulum
$GABA_BR$	Gamma-aminobutyric acid type B receptor
GIRK	G-protein coupled inward rectifier potassium channel
HEK293T cells	Human embryonic kidney 293T cells
ICL2	Intracellular loop 2
ICL3	Intracellular loop 3
IHC	Immunohistochemical staining
IP	Immunoprecipitation
IP_3R	Inositol 1,4,5-trisphosphate receptor
IVM	Ivermectin
K_{ir}	Inward rectifier potassium channels
M2R	Muscarinic acetylcholine receptor M2
M4R	Muscarinic acetylcholine receptor M4
MAM	Mitochondrion-associated endoplasmic reticulum membrane
mGluR2	Metabotropic glutamate receptor 2
NMDAR	N-methyl-D-aspartate receptor
N-ter	N-terminal
OXO-M	Oxotremorine-M
PLL	Poly-L-Lysine
PM	Plasma membrane
S1R	Sigma-1 receptor
SBLD I	Steroid-binding-like domain I
SBLD II	Steroid-binding-like domain II
SKF10047	(+)-N-Allylnormetazocine hydrochloride
STIM1	Stromal interaction molecule 1
TM	Transmembrane domain
TRPV1	Transient receptor potential cation channel subfamily V member 1
WT	Wild type

Summary

Sigma-1 receptor (S1R) is a multimodal chaperone protein located chiefly at the mitochondrion-associated endoplasmic reticulum (ER) membrane (MAM) at rest. S1R can translocate to various regions of the cell such as plasma membrane (PM) or ER-PM junction under cellular stress or the application of its ligands. It has been implicated in a diverse array of pathophysiological conditions including drug addiction, Parkinson's disease, Alzheimer's disease and amyotrophic lateral sclerosis (ALS). One of the well-known disease associated mutants of S1R, called ALS-linked E102Q mutation, is reported to cause ER stress-mediated defects in protein homeostasis and dysregulation of RNA-binding proteins, eventually leading to the occurrence of ALS. The crystal structure analysis of human S1R revealed that S1R has only one transmembrane domain (TM) with a short N-terminal (N-ter) on the luminal side and a bulky C-terminal (C-ter) including a β-barrel structure on the cytosolic side. The site of the E102Q mutation locates on the C-ter of S1R. It has been reported that S1R directly interacts with various proteins such as NMDAR, STIM1, BiP, IP_3R, voltage-gated K^+ and Na^+ channels. It was also reported that S1R colocalizes with muscarinic acetylcholine receptor M2 (M2R) on the soma of motoneurons. M2R is one of the Gi/o coupled receptors expressed on PM of such as cardiac muscle cells and neurons, and it plays key roles in wide-ranged physiological responses. Despite of the knowledge of the colocalization of M2R and S1R, there is no information about the functional regulation of M2R by S1R so far.

The aim of the first part of this study is to clarify whether and how S1R could interact with M2R, and I obtained the results as follows: (1) By patch-clamp recordings of HEK293T cells coexpressing G-protein coupled inward rectifier potassium channel (GIRK) as an effector, it was observed that S1R inhibits the function of only M2R among other types of $G_{i/o}$ coupled receptors. But the S1R disease mutant E102Q does not inhibit the function of M2R. (2) By immunohistochemical staining and confocal imaging, it was observed that the expression level of M2R on PM is not clearly down regulated by S1R in HEK293T cells, and that of M2R on PM is slightly decreased by S1R in Hela cells. In both HEK293T and Hela cells, S1R localizes close to

M2R, suggesting an interaction with M2R at the ER-PM junction. (3) By co-immunoprecipitation, the interaction of M2R and S1R was confirmed. (4) By analyzing various chimeras and mutants between M2R and M4R, it was identified that Glu172 and Glu175 of M2R on the extracellular loop 2 region, as well as transmembrane domain 6 (TM6), are critical for the inhibition by S1R. The data demonstrate that S1R, not only decreases the expression level on the PM, but also inhibits the function of M2R, via the extracellular loop 2 and TM6.

Based on the preceding pharmacological studies, S1R is presumed to exist in various forms from monomer to octamer, and the functional forms of S1R are monomer and dimer. Agonist bound S1R favors monomeric or dimeric forms, while antagonist bound S1R favors tetrameric form which loses its function. BD1047 dihydrobromide (BD1047) is one of the representative antagonists of S1R. I have tried to inhibit the function of S1R using BD1047 in the patch-clamp study, and unexpectedly observed that BD1047 directly inhibits the GIRK1/2 current even without the expression of S1R.

In the second part, I aimed to clarify the effect of BD1047 on GIRK channels as well as the structural determinants. I performed two-electrode voltage clamp experiments using Xenopus oocytes as in vitro expression system and observed the following results: (1) BD1047 directly inhibits the current of GIRK channels. (2) BD1047 has a weak inhibition effect on GIRK2 channel and a remarkable inhibition effect on GIRK4 channel. (3) A GIRK4-GIRK2 chimera which contains only the cytoplasmic N-ter of GIRK4 showed a strong inhibition effect by BD1047. Leu77 on the N-ter of GIRK4 is essential for the inhibition effect. (4) Molecular docking analysis indicated the importance of the Leu77 for the docking. The data demonstrate that BD1047 directly inhibit the current of GIRK channels and GIRK4 Lue77 is essential for the inhibition effect by BD1047.

To summarize all the data, it is concluded that S1R partly decreases the expression of M2R on PM and also inhibits its function via its extracellular loop 2 and TM6, and that the antagonist of

S1R, BD1047, directly binds to GIRK4 channel and inhibits the current at Leu77 in the N-ter cytoplasmic region.

Introduction

Sigma-1 receptor (S1R) has been recognized as opioid receptor and it is a chaperone protein which is mainly expressed in the brain and liver (Chu & Ruoho, 2016; Su *et al.*, 2016). It has been extensively studied in the physiological and pathophysiological processes in the central nervous system such as pain, memory, Parkinson's disease, Alzheimer's disease and also juvenile amyotrophic lateral sclerosis (ALS) in which the E102Q mutation of S1R is involved (Dreser *et al.*, 2017). Within the cell, S1R is located chiefly at the mitochondrion-associated endoplasmic reticulum membrane (MAM) region at rest and plays important roles in supporting the IP_3 receptor (IP_3R) to maintain the Ca^{2+} homeostasis between endoplasmic reticulum (ER) and mitochondria (Hayashi & Su, 2007).

Molecular architecture of Sigma-1 receptor

S1R was originally proposed to have two hydrophobic helical transmembrane domains (TMs) by the sequence-based algorithms including amino acid hydrophobicity analyses and structural flexibility assessment plots (Chu & Ruoho, 2016). Based on this two-TMs model, both N-and C-terminal of this receptor were assumed to be located in the lumen side of ER. In addition, the C-terminal (C-ter) of S1R has been demonstrated to be the ligand binding side containing steroid-binding-like domains II (SBLD II) (Ortega-Roldan *et al.*, 2013). This proposed structure has been supported by NMR analysis of the S1R construct whose first 35 amino acids in the N -terminal (N-ter) were deleted (Ortega-Roldan *et al.*, 2015) **(Fig. 1A)**.

In contrast to the two TMs model of S1R, the first crystal structure of human S1R revealed a trimeric architecture with only one TM in each protomer (Schmidt *et al.*, 2016). In this structure model, the position of the C-ter containing a cupin-like β-barrel, which is referred to as the ligand binding site, is located on the cytosolic side in contrast to the previous findings **(Fig. 1B)**.

Thus, the two distinct structure models of S1R proposed by different experimental methods have brought the structure of this receptor controversial. The topology of the crystal structure is

more likely, as the ligand binding domain in the C-ter is located on the cytosolic side. The trimeric structure, however, might be due to the specific form in the crystal, apart from that in the functioning state. Since a precise S1R structure is essential for the research design towards the understanding of its function, further investigations to reveal the structure in function are required.

Function and ligands of Sigma-1 receptor

Different oligomerization states from monomer to octamer of S1R have been reported (Gromek *et al.*, 2014; Mishra *et al.*, 2015). It was proposed that S1R functions in its lower oligomeric forms such as monomer and dimer to interact with its client proteins. Agonists of S1R make S1R stay in monomer or dimer forms and maintain its function, and antagonists of S1R disrupt the function of S1R by keeping it in its higher oligomer forms (Chu & Ruoho, 2016) **(Fig. 2)**.

The ligand binding domains of S1R have been determined by S1R protein purification and the use of photo-affinity labels and they are called SBLD I and SBLD II which locate in the center of a cone-shaped β-barrel of the C-ter of S1R (Pal *et al.*, 2007; Fontanilla *et al.*, 2008). Meanwhile, various structurally diverse compounds have been identified to bind to S1R with a high affinity at the SBLD I and SBLD II regions. Clinically used drugs such as pentazocine, cocaine and fluvoxamine are known as agonists of S1R and progesterone, haloperidol are known as antagonists. Synthetic agonist and antagonist of S1R, (+)-N-Allylnormetazocine hydrochloride (SKF10047) and BD1047 dihydrobromide (BD1047), were also identified (Su *et al.*, 2010). However, the endogenous ligands of S1R in physiological processes remain unidentified.

Translocation of Sigma-1 receptor upon ligand binding

The location of S1R in the MAM region is widely accepted. However, accumulated studies showed that the S1R dynamically redistributes to the plasma membrane (PM) and the nuclear envelope under some conditions, such as pharmacological treatments or during cellular stresses (Mavlyutov & Ruoho, 2007). The application of S1R agonist such as (+) pentazocine, is known to initiate the

dissociation of S1R from the regular binding partner immunoglobulin binding protein (BiP) on the ER membrane and causes the translocation of S1R from the MAM (Hayashi & Su, 2003). It is reported that the application of pentazocine causes the reduction of S1R in the lipid raft fraction, with a dramatical move to the non-raft fraction. Mounting evidences have demonstrated the importance of the lipid raft microdomain in the regulation of the subcellular distribution of S1R (Chu & Ruoho, 2016).

Interaction between various types of proteins and Sigma-1 receptor

S1R is a well-known multimodal chaperone protein and cumulative studies demonstrated that it can directly/indirectly interact with and regulate the function of various types of membrane proteins such as IP_3R, stromal interaction molecule 1 (STIM1), some ion channels, N-methyl-D-aspartate receptor (NMDAR) (Su *et al.*, 2016; Sabeti *et al.*, 2007; Mavlyutov *et al.*, 2010). For instance, S1R is reported to diminish the current amplitude and accelerate the inactivation phase of $K_v1.4$ channel upon depolarization. Moreover, the application of its agonist SKF10047 could further decrease the total current of $K_v1.4$ channel (Aydar *et al.*, 2002). Meanwhile the underlying mechanisms are not explicitly known. There are two aspects of the underlying mechanisms remaining to be elucidated. One is that, where and how the S1R interacts with ion channels after the redistribution of S1R by application of its agonists. The interaction might occur on the PM in the side-by-side manner or still within the cell but close to the PM like ER-PM junction in the head-to-tail manner **(Fig. 3)**. The other is that the elusive structural determinants are needed to be identified, e.g. the binding site for ligands and the coupling site for ion channels.

Muscarinic acetylcholine M2 receptor (M2R) is one of the Gi/o coupled receptors on the PM known to play important roles in the regulation of activities of cardiac muscle cells and neurons. S1R has been reported to colocalize with M2R on the soma of motoneurons in the mouse brainstem and spinal cord by immunohistochemical staining (IHC) **(Fig. 4A)**. The images at the electron microscope level demonstrated that S1R locates on the surface of ER, but not on the plasma

membrane (Mavlyutov *et al.*, 2010) **(Fig. 4B)**. Although M2R and S1R showed colocalization and they may locate on PM and ER, respectively, it is still possible that S1R directly regulates the function of M2R via protein-protein interactions presumably at the ER-PM junction if the distance between them is short enough. Despite the observation that M2R and S1R colocalize together, there is no study so far focusing on the functional aspect. If S1R could regulate the function of M2R, it is also necessary to reveal the underlying molecular mechanisms, i.e. where and how do they interact with each other.

Materials and Methods

Ethical approval

All animal experiments in this study were approved by the Animal Care Committee of the National Institutes of Natural Sciences (an umbrella institution of National Institute for Physiological Sciences, Japan), and were performed in accordance with its guidelines.

Cell culture and transfection

Plasmids of GIRK1/2 (1μg), M2R (1μg) and S1R (1μg) were transfected to human embryonic kidney 293T (HEK293T) cells or Hela cells using Lipofectamine 2000 reagent (Invitrogen) following the protocol by suppliers for patch-clamp experiments and immunohistochemical staining. Plasmids of M2R (2μg) and S1R (2μg) were transfected to HEK293T cells using Avalanche-Everyday Transfection Reagent (Avalanche®- Everyday) for co-immunoprecipitation following the protocol by suppliers. After 36-48 h of the transfection, cells were re-seeded onto Poly-L-Lysine (PLL) coated glasses for patch-clamp recording, or fixed for immunohistochemical staining.

Preparation of *Xenopus laevis* oocytes

Oocytes were isolated from *Xenopus laevis* (purchased from Hamamatsu Seibutsu Kyouzai, Hamamatsu, Japan) under anesthesia of 0.15% tricaine (Sigma-Aldrich) by surgery. Surgical operation of frog was performed on ice and an incision was made in the frog's abdomen to take out the oocytes. The isolated oocytes were incubated in 2 mg mL^{-1} collagenase type I (Sigma-Aldrich) for 6 hours to remove the follicular membrane and stored in frog Ringer's solution containing 88 mM NaCl, 1 mM KCl, 2.4 mM $NaHCO_3$, 0.3 mM $Ca(NO_3)_2$, 0.41 mM $CaCl_2$, 0.82 mM $MgSO_4$ and 15 mM Hepes with 0.1% penicillin-streptomycin at 17 °C. After the injection of the 50 nL of cRNA, oocytes were incubated in frog Ringer's solution for 3-4 days for electrophysiological recordings.

Mutagenesis and cDNA and cRNA preparations

In the experiments in HEK293T cells, the cRNAs of wild type (WT) human S1R and S1R E102Q cDNA with V5- and histidine-tag, S1R with EGFP-tag in pcDNA3.1(-), provided by Dr Ruth Murrell-Lagnado (University of Sussex, Brighton, UK), were used. The cDNA of porcine M2R, porcine M2R-CFP, rat M4R, $GABA_BR$ and mGluR2 and GIRK1/2 were all subcloned into pcDNA3.1(-). Mutations in M2R and M4R were introduced using the PfuUltra II Fusion HS DNA Polymerase kit (Agilent Technologies) and verified by DNA sequencing. M2R-EGFP construct was made by incorporating the EGFP at the end of M2R WT using the PfuUltra II Fusion HS DNA Polymerase kit (Agilent Technologies), and was subcloned into NotI and EcoRI site of pcDNA3.1(-) and then verified by DNA sequencing.

In the experiments in Xenopus oocytes, cDNAs of WT mouse GIRK2 and WT rat GIRK4 subcloned into pGEMHE were used. Mutations in mouse GIKR2 and rat GIRK4 were introduced using the PfuUltra II Fusion HS DNA Polymerase kit (Agilent Technologies) and verified by DNA sequencing. After linearization of cDNA by restriction enzymes, complementary RNAs were transcribed using mMessage mMachine kit (Ambion). The cRNAs of mouse GIRK2 (4.15 ng $oocyte^{-1}$), rat GIRK4 (4.15 ng $oocyte^{-1}$), bovine G-protein β1 (4.15 ng $oocyte^{-1}$) and bovine G-protein γ2 (4.15 ng $oocyte^{-1}$) were injected to the oocytes.

Electrophysiological recording

In the whole cell patch clamp recording from HEK293T cells, data were acquired using patch clamp amplifier (AXOPATCH 200B), a digital analogue converter (Digidata 1440A, Molecular Devices) and pCLAMP 10.7 software (Molecular Devices). HEK293T cells were attached to PLL coated glass 4-6 hours before recording and placed in the recording chamber, and membrane current were recorded under whole cell patch clamp using a glass micropippette with the access resistance of 3-5MΩ when filled with 140 mM KCl, 5 mM Na_2-ATP, 3 mM EGTA, 0.1 mM $CaCl_2$, 10 mM HEPES, 5 mM $MgCl_2$ (PH 7.3 with KOH). 140K^+ solution (140 mM KCl, 4 mM NaCl,

1mM $CaCl_2$, 0.3 mM $MgCl_2$ and 10 mM Hepes, pH 7.4 with KOH) or 140Na^+ solution (140 mM NaCl, 4 mM KCl, 0.3 mM $MgCl_2$, 1 mM $CaCl_2$ and 5 mM Hepes, pH 7.4 with NaOH) were used as an extracellular solution for recordings. All experiments were performed at 25-28 °C. Ligands, 50 μM OXO-M, 100 μM GABA, 200 μM Glutamate and 50 μM BD1047 with 50 μM OXO-M in 140K^+ were delivered and wash out by gravity flow using a muti-valve controller system (VC-8 VALVE CONTROLLAER, warner instruments).

In the two electrodes voltage clamp recording from Xenopus oocytes, data were acquired by Oocyte clamp amplifier (OC-725C, Warner Instruments), a digital analogue converter (Digidata 1550A, Molecular Devices) and pCLAMP 10.5 software (Molecular Devices). An oocyte was placed in the recording chamber and membrane current were recorded under voltage clamp using two glass microelectrodes with the resistance 0.1-0.5 MΩ when filled with 3 M potassium acetate with 10 mM KCl. 96K^+ solution (96 mM KCl, 3 mM $MgCl_2$ and 5 mM Hepes, pH 7.5 with KOH) or ND96 solution (96 mM NaCl, 2 mM KCl, 1 mM $MgCl_2$, 1.8 mM $CaCl_2$ and 5 mM Hepes, pH 7.5 with NaOH) were used as an extracellular solution for recordings. All experiments were performed at 25-28 °C. Various concentrations of BD1047 were applied and wash out by perfusion using a peristaltic pump (AC-2110 II, ATTA).

Immunohistochemical staining

HEK293T or Hela cells were fixed with 4% paraformaldehyde in PBS for 10 min at room temperature, blocked in 2% skim milk with 0.1% Triton X-100 in PBS, and then incubated with the primary antibody diluted in PBS. A rabbit polyclonal anti-EGFP antibody (Invitrogen, 1:200 dilution) and a mouse monoclonal anti-V5 tag antibody (Invitrogen, 1:500 dilution) were used. After the primary antibody, the sample were incubated with the secondary antibody conjugated with Alexa Fluor-488 (Invitrogen, dilution 1:500) or Alexa Fluor-568 (Invitrogen, 1:500 dilution).

Co-immunoprecipitation

HEK293T cells were cultured in 60mm dishes until cells reach 80-90% confluency and then were co-transfected with M2R-EGFP and S1R-V5-His using the Avalanche-Everyday Transfection Reagent (Avalanche®- Everyday) following the protocol of the supplier. Cells were lysed after 48 hours of incubation. Cell lysate was preincubated with G-Sepharose (Protein G Sepharose™ 4 Fast Flow, GE Healthcare) in a rotating wheel for 1hr at 4°C and then were centrifuged to remove the G-Sepharose and the supernatant was collected. Then, mouse monoclonal anti-EGFP antibody (Sigma-Aldrich, 2µg) for immunoprecipitating M2R or mouse monoclonal anti-V5 tag antibody (Invitrogen, 2µg) for immunoprecipitating M2R was added to the supernatant with G-Sepharose and incubated in a rotating wheel for 2 hours at 4°C. After 2 hours of rotating incubation, samples were washed by wash buffer and centrifuged 3 times repeatedly. Wash buffer was completely removed following the final centrifuge, and the sample buffer containing SDS was added to the tubes and heated for 5 mins at 95°C. Proteins were finally analyzed by western blot.

Western blot analysis

Total protein lysate and IP samples were separated by SDS/PAGE (SuperSep^{TM}Ace, 10-20%, 13 or 17well, FUJIFILM) and blotted to PVDF membranes (Sigma-Aldrich) by using wet transfer system. Membranes were blotted by Blocking One (Nacalai Tesque Inc.) and then incubated with monoclonal rabbit anti-M2R antibody (Abacm, dilution 1:1000) or polyclonal rabbit anti-His tag antibody (Bethyl Laboratories, dilution 1:1000) diluted in Blocking One solution for 1 hour at room temperature. Membranes were then washed by PBST for 3 times, and samples were incubated with anti-rabbit secondary antibody conjugated with horseradish peroxidase (GE Healthcare, dilution 1:5000) to visualize and detected by chemiluminescence (ImmunoStar zeta kit, FUJIFILM).

Molecular docking

Homology model of GIRK4 was built based on the structure of GIRK2 (6XIT, RCSB protein data bank) using SWISS-MODEL (https://swissmodel.expasy.org/). The dimer form of GIRK4 was made from the homology model of GIRK4 using PyMOL software. Chemical structure of BD1047 was downloaded from the website. The dimer form of GIRK4 and the structure of BD1047 were uploaded to SwissDock (http://www.swissdock.ch/) to obtain the docking results. The computational docking results was presented with color marks using Chimera 1.16 software.

Chemicals

OXO-M was purchased from Sigma-Aldrich and dissolved in distilled water to make a 50 mM stock solution and further diluted in the bath solution for the final concentration 50 μM. BD1047 was purchased from Tocris Bioscience and dissolved in distilled water to make a 50 mM stock solution and further diluted in the bath solution for the final concentrations from 0.1μM up to 500 μM. Sources of other materials are described in the relevant methods.

Data analyses

In the patch-clamp experiments, all data were analyzed by Clampfit 10.7 (Molecular Devices) and Igor 5 (WaveMetrics) and are shown as mean ± SD from n single HEK293T cells. The current recorded in 140 Na^+ was subtracted to remove the endogenous current from HEK293T cells. The current amplitude of GIRK1/2 channel was recorded at -120mV before and after the application of the agonists to various $G_{i/o}$ coupled receptors. Activation ratio of GIRK1/2 channel by various agonists was calculated by the current amplitude in the presence and absence of the ligand after subtraction of endogenous current in 140 Na^+ ($I_{GIRK\ agonist\ (+)}$ /$I_{GIRK\ agonist\ (-)}$). Activation ratio of 1 means there was no change in the current amplitude after the application of agonists.

In the two-electrode voltage clamp experiments, all data were analyzed by Clampfit 10.7 (Molecular Devices) and Igor 5 (WaveMetrics) and are shown as mean ± SD from n single oocytes.

The current amplitude of GIRK channel was recorded at -100mV before and after the application of BD1047. The inhibition percentage of GIRK current by BD1047 was calculated by the decrease in the current amplitude in the presence of 100 μM BD1047 from the current before its application at -100 mV ($I_{GIRK\ basal}$ -$I_{GIRK\ BD1047\ (+)}$ / $I_{GIRK\ basal}$), and the basal current amplitude after subtraction of the current in ND96 solution was normalized as 100%. The dose-inhibition relationship was analyzed by sequential application of various concentrations of BD1047. By using Igor, the data were fitted to a Hill equation: y = min + (max − min) / (1 + (x/IC_{50}) ^ (Hillslope)).

All experiments were performed with the number of n ≥ 4 for each group. Statistical significances of differences were evaluated using Tukey's multiple comparison tests following one-way ANOVA or Student's *t*-test (unpaired). The values of $P<0.05$ were judged to be statistically significant.

Results

Part I

Regulation of M2R by S1R and S1R disease mutant E102Q

It has been demonstrated that M2R is colocalized with S1R at the postsynaptic site of motoneurons in the ventral horn in the mouse brainstem and spinal cord (Mavlyutov *et al.*, 2010), but the functional relationship between them has not been explored yet. As the initial step, I examined whether S1R regulates the function of M2R or not. By using HEK293T cells as an in vitro expression system, G-protein coupled inward rectifier potassium channel 1/2 (GIRK1/2) and M2R with or without S1R were expressed in HEK293T cells. The reasons to co-express GIRK1/2 channel are that M2R belongs to Gi/o coupled receptor family, that GIRK1/2 channel is an effector of Gi/o coupled receptor, and that the activity of M2R could be measured by the change of the current amplitude of GIRK1/2 channel (Wickman & Clapham, 1995). Upon the application of oxotremorine-M (OXO-M), one of the synthetic agonists of M2R, current amplitude of GIRK1/2 channel increases due to the binding of $G_{\beta\gamma}$ subunits which are dissociated from Gi/o upon activation of M2R (Logothetis *et al.*, 1987; Mistry *et al.*, 2005).

In the GIRK1/2 and M2R transfected group, it was observed that the change of the bath solution from 140 K^+ to 140 K^+ with OXO-M could evoke a remarkable increase in the GIRK1/2 current **(Fig. 5B)**, while it could not be clearly observed in the presence of S1R **(Fig. 5C)**. The increase fold of the GIRK1/2 current amplitude was 7.0±3.4 in the absence of S1R and 0.9±0.6 in its presence **(Fig. 7B)**. Meanwhile, there was no difference in the basal current amplitude of GIRK1/2 before application of OXO-M between both groups showing that S1R does not affect the expression and function of GIRK1/2 channel itself **(Fig. 7A)**. This indicates that the expression of S1R inhibits the expression and/or function of M2R.

A disease associated mutant of S1R, called ALS-linked S1R E102Q mutation, is known to induce ER stress-mediated defects in protein homeostasis and dysregulation of RNA binding proteins which eventually causes the occurrence of ALS (Dreser *et al.*, 2017). It is interesting to

examine whether or not this S1R E102Q could affect the function of M2R. Similar results showing M2R activation were obtained in both of the GIRK1/2 and M2R co-transfected groups with or without S1R E102Q. Both groups showed OXO-M evoked further increase in the GIRK1/2 current, indicating that S1R E102Q does not inhibit the function of M2R **(Fig. 6B, C)**. OXO-M induced increase in the GIRK1/2 current via M2R was 4.4±1.4 fold in the absence of S1R E102Q and it was 5.3±2.6 fold in the presence. There was no significant difference in the increase ratio of the GIRK1/2 current between the two groups (**Fig. 7B)**. This shows that the inhibition effect on M2R is lost in S1R E102Q and the function of M2R cannot be regulated by the S1R disease mutant. Taken together, these data demonstrate that function of M2R can be inhibited by S1R, but not by the S1R disease associated mutant E102Q.

Regulation of M2R and other types of $G_{i/o}$ coupled receptors by S1R

Besides M2R, there are various $G_{i/o}$ coupled receptors, for example, muscarinic acetylcholine receptor M4 (M4R), gamma-aminobutyric acid type B receptor ($GABA_BR$), metabotropic glutamate receptor 2 (mGluR2). They share a similar downstream signaling pathway after stimulation by their ligands (Fredriksson *et al.*, 2003). In order to examine the effect of S1R on other types of $G_{i/o}$ coupled receptors, experiments to co-transfect various $G_{i/o}$ coupled receptors with S1R in HEK293T cells were conducted. M2R, M4R, $GABA_BR$ or mGluR2 are co-transfected with or without S1R, and their agonists OXO-M, GABA or glutamate were applied during recording. The results again showed a clear inhibition effect of S1R on M2R. In the case of M4R, the increase ratios of current amplitude of GIRK1/2 by OXO-M without or with S1R were 4.5±1.4 and 3.9±0.8 fold, respectively. As to $GABA_BR$, the activation ratios of GIRK1/2 current by GABA without or with S1R were 2.7±1.0 and 2.1±0.7 fold, respectively. In the case of mGluR2, the activation ratios of GIRK1/2 current by glutamate without or with S1R were 5.7±2.7 and 6.2±2.2 fold, respectively. There were no significant differences of the activation ratios of GIRK1/2 current in the absence and presence of S1R in M4R, $GABA_BR$ and mGluR2 groups **(Fig. 8)**. In conclusion,

S1R has no inhibition effect on M4R, $GABA_BR$ and mGluR2, and the inhibition effect of S1R on M2R is unique among other types of Gi/o coupled receptors.

Immunohistochemical staining of M2R and S1R in HEK293T and Hela cells

There are two possibilities about how S1R inhibits the function of M2R. One possibility is that S1R retains M2R within the cell and thereby reduces the surface expression of M2R on PM. The other possibility is that S1R directly binds to M2R on PM and regulates its function. To examine these possibilities, it is important to confirm the surface expression level of M2R. Towards this aim, IHC of M2R and S1R were performed using HEK293T cells as they were used for the electrophysiological analyses. For better special discrimination of PM and ER, Hela cells which are flatter and wider were also used. All images were obtained by confocal microscope.

V5 tagged S1R and CFP tagged M2R constructs were used in all experiments. The red fluorescence signal represents the expression of M2R and the green fluorescence signal represents the expression of S1R. In HEK293T cells, the expression of M2R on PM in the absence and presence of S1R did not show clear difference **(Fig. 9A, B)**. The results show that the expression level of M2R on PM is not clearly down regulated by S1R, suggesting that the inhibition effect of S1R on M2R is due to chiefly functional inhibition. In Hela cells, the expression of M2R on PM was slightly decreased in the presence of S1R, but significant expression of M2R on PM was still clearly observed **(Fig. 10A, B)**. Meanwhile, the expression of M2R was clearly decreased in the presence of S1R E102Q **(Fig. 10C)**. The results show that the inhibition effect on M2R might be partly due to the down regulation of the expression of M2R on PM as well as the functional inhibition of the remained M2R on PM by S1R, and that the S1R E102Q down regulates the expression of M2R on PM.

To examine if M2R and S1R are colocalized together, the red fluorescence signal from M2R and the green fluorescence signal from S1R were overlaid in co-transfected HEK293T and Hela cells. It was shown that M2R locates more on PM and S1R locates chiefly on ER. The overlaid

yellow signal indicates colocalization of M2R and S1R within the HEK293T or Hela cells, but not on the PM. It was shown that M2R and S1R are closely located together, and that they may interact with each other within the HEK293T or Hela cells presumably at the ER-PM junction **(Figs. 9C, 10B)**. In Hela cells, it was observed that S1R E102Q is remarkably clustered at the ER adjacent to the nucleus where it colocalizes with M2R **(Fig. 10C)**.

To better evaluate the subcellular localization of S1R, S1R and ER were stained at the same time in Hela cells. S1R was detected by anti-V5 tag antibody and stained in green fluorescence signal. Since calnexin is an integral ER protein and can be used as ER marker, ER was detected by anti-calnexin antibody and stained in red fluorescence signal. It was observed in the overlaid images that S1R is almost fully overlapped with ER marker, showing S1R is expressed on ER in Hela cells transfected with S1R alone or co-transfected S1R with M2R **(Fig. 11A, B)**. In Hela cells co-transfected S1R E102Q with M2R, on top of the intense expression of S1R E102Q in ER adjacent to nucleus, spread to regions other than ER was observed **(Fig. 11C).**

Taken together, the expression of M2R on PM in HEK293T cells is not clearly down regulated by S1R, but that it was slightly down regulated by S1R in Hela cells. S1R is expressed on ER, and it is likely that M2R and S1R are colocalized presumably at the ER-PM junction in both HEK293T and Hela cells.

Co-immunoprecipitation of M2R and S1R

As a next step, the protein-protein interaction between M2R and S1R was examined by co-immunoprecipitation analysis. M2R was tagged with EGFP (M2R-EGFP), and S1R was tagged with V5 and His tags (S1R-V5-His). The predicted molecular weights of M2R and S1R including tags are 78.6kDa and 27.2kDa, respectively. M2R-EGFP and S1R-V5-His were co-transfected in HEK293T cells. M2R was precipitated by anti-EGFP mouse antibody and S1R was precipitated by anti-V5 tag mouse antibody. In the immunoblotting, M2R was detected by anti-M2R rabbit antibody and S1R was detected by anti-His tag rabbit antibody.

Cell lysate samples clearly showed the expression of M2R and S1R with predicted band sizes, and the sample of the M2R immunoprecipitation (IP) showed a successful precipitation of M2R of the indicated size. Meanwhile, it was also shown that S1R of the predicted size co-precipitated with M2R **(Fig. 12A)**. As a negative control, S1R was transfected alone in HEK293T cells and was precipitated by anti-EGFP tag mouse antibody which is used for precipitation of M2R. S1R could be detected in the cell lysate but not in the IP sample **(Fig. 12C)**. The sample of the S1R IP showed a successful precipitation of S1R, and also co-precipitation of M2R with S1R was detected **(Fig. 12B)**. As a negative control, M2R was transfected alone in HEK293T cells and was precipitated by anti-V5 tag mouse antibody which is used for precipitation of S1R. M2R could be detected in the cell lysate but not in the IP sample **(Fig. 12D)**. Taken together, it was observed that S1R co-precipitates with M2R and that M2R co-precipitates with S1R, demonstrating the protein-protein interaction between M2R and S1R.

Regulation of M2R/M4R chimeras and M2R mutants E172P/E175Q by S1R

Although it was confirmed that S1R inhibits the function of M2R and that they indeed directly interact with each other, the underlying mechanism remains unclear. Thus, it is needed to reveal the structural determinants of the inhibition of M2R by S1R.

M2R and M4R both belong to the muscarinic cholinergic receptor family, and share a high similarity of the amino acid sequences, whereas the inhibition of S1R on them is distinguishable **(Fig. 8)**. Taking advantage of the different inhibition effects of S1R on them, chimeras between M2R and M4R were made in order to identify the structural determinants for the interaction between M2R and S1R **(Fig. 13)**. M2R chimeras which contain the whole intracellular loop 3 (ICL3), N-ter to intracellular loop 2 (ICL2) or C-ter of M4R still exhibited inhibition effects by S1R, suggesting that all these parts of M2R are not involved in the inhibition by S1R **(Fig. 14)**. Therefore, the remaining part from TM4 to TM7 might be critical for the interaction with S1R.

In the TM4-7 region, I first made a chimera swapping TM4-5 between M2R and M4R (**Fig.13**) and it was observed that M2R/M4R(TM4-5) chimera lost the inhibition effect by S1R **(Fig. 14)**. This suggested that TM4-5 of M2R may be involved in the inhibition effect by S1R. Thus, I focused on the TM4-5 region of M2R and compared the amino acid sequence of M2R and M4R, and found only a few differences of amino acids. Therefore, single point mutants of Val168, Glu172, Glu175 and Phe181 of M2R to the corresponding amino acid Lys, Pro, Gln and Leu of M4R (M2R V168K, M2R E172P, M2R E175Q, M2R F181L) were made **(Fig. 15)** and analyzed electrophysiologically. The position of Glu172 and Glu175 on the extracellular loop 2 of M2R were identified to be critical for the inhibition of M2R by S1R. In the experiments of M2R E172P mutant, no matter co-transfection with S1R or not, OXO-M could induce further increase in GIRK1/2 current through M2R **(Fig. 16B, C)**. The activation ratios were 6.9±4.8 fold in the absence of S1R and 4.3±1.7 fold in its presence **(Fig. 18A)**. As for the M2R E175Q mutant, a similar phenomenon to M2R E172P, lack of inhibition by S1R, was observed **(Fig. 17B, C)**. The activation ratios were 5.2±1.7 fold in the absence of S1R, and 5.3±2.2 fold in its presence **(Fig. 18A)**. There were no statistically significant differences in the activation ratio with or without S1R in both groups **(Fig. 18A)**. As expected, the double mutant of M2R, E172P/E175Q, also lost the inhibition effect by S1R **(Fig. 18A)**. These results demonstrate that Glu172 and Glu175 on the extracellular loop of M2R between TM4 and TM5 play critical roles in the inhibition of M2R by S1R **(Fig. 18B, C)**.

Regulation of M2R/M4R TM6-7 chimeras by S1R

Although Glu172 and Glu175 on the extracellular loop of M2R were identified as critical sites for the inhibition effects by S1R, the reverse mutants of M4R, P180E, Q183E and P180E/183E did not show inhibition effect by S1R. Mutants such as M4R P180E/N182G/Q183E, P180E/Q183E/F185Y and P180E/N182G/Q183E/F185Y did not either acquire the inhibition effect by S1R (**Fig.19**). The results indicate that Glu172 and Glu175 on M2R are important for the inhibition of M2R by S1R,

but their presence is not sufficient. Therefore, it is speculated that there might be other critical site(s) in M2R.

In the study of chimeras between M2R and M4R, the TM6 to TM7 region remained untouched. Thus, the chimeras swapping the TM6 and TM7 between M2R and M4R were made **(Fig. 20)**. The expression of S1R did not inhibit the OXO-M induced GIRK1/2 current via M2R/M4R(TM6) which contains the TM6 from M4R **(Fig. 21B, C)**. On the other hand, S1R did inhibit the function of M4R/M2R(TM6) **(Fig. 22B, C)**. However, swapping of the TM7 between M2R and M4R does not change the inhibition effect by S1R showing that TM7 is not critical **(Fig. 23)**. Statistical analyses showed that M4R/M2R (TM6) has a significant inhibition effect by S1R like M2R WT and M2R/M4R (TM6) lacks the inhibition effect by S1R like M4R WT **(Fig. 23)**. Thus, it was demonstrated that TM6 of M2R is also critical for the interaction between M2R and S1R.

Part II

Inhibition of GIRK channels by BD1047

In the initial stage of the study to examine whether S1R can regulate the function of M2R, I also tried to block the function of S1R using the known antagonist of S1R, BD1047 **(Fig. 24A)**. In the HEK293T cells transfected with GIRK1/2, M2R and S1R, the application of BD1047 suppressed the OXO-M induced GIRK1/2 current **(Fig. 24C)**. The application of BD1047 also suppressed the OXO-M induced GIRK1/2 current even in the absence of S1R **(Fig. 24B)**. The results show that BD1047 might has a direct inhibition effect on GIRK channel. For the sake of high throughput experiments, Xenopus oocytes were used as an in vitro expression system and two-electrodes voltage clamp experiments were performed to examine this possibility.

GIRK channel has four subfamily members which are GIRK1, GIRK2, GIRK3 and GIRK4, and they form functional homotetramers or heterotetramers. For example, the GIRK1/2 heterotetramer is expressed in the brain and regulates neuronal excitability and the GIRK1/4 heterotetramer is expressed in the heart and regulates the heart rate (Hibino *et al.*, 2010). The effect

of BD1047 on the heteromeric GIRK1/2 and GIRK1/4, the homomeric GIRK2 and GIRK4 were examined without co-expression of M2R and S1R. Since homo GIRK4 channel shows a small basal current (Hibino *et al.*, 2010), its physiological activator $G_{\beta\gamma}$ subunits were co-expressed together with GIRK4 in order to clearly observe the GIRK4 current. The application of BD1047 decreased the current amplitude of GIRK1/2, GIRK2, GIRK1/4 and GIRK4 to various degrees **(Figs. 25, 26)**. The inhibition percentages were 51.0±1.8%, 37.7±9.8%, 47.4±4.9% and 79.9±4.6% for GIRK1/2, GIRK2, GIRK1/4 and GIRK4, respectively **(Fig. 27)**. Therefore, it was confirmed that BD1047 directly inhibits the current amplitude of GIRK channels, especially that of GIRK4.

Inhibition of GIRK2/4 chimeras by BD1047

It was found that BD1047 has a weak inhibition effect on GIRK2 channel and a strong inhibition effect on GIRK4 channel **(Fig. 27)**. As a next step, the dose response relationship of BD1047 on GIRK2 or GIRK4 current was analyzed. GIRK2 was also co-expressed with $G_{\beta\gamma}$ subunits to ensure the same experimental conditions as GIRK4 **(Fig. 28A)**. The IC_{50} of BD of GIRK2 was 75.4 ± 9.7 μM and that of GIRK4 was 17.4 ± 3.7 μM **(Fig. 28B)**, confirming that GIRK4 is more sensitive to the block by BD1047 than GIRK2. The Hill efficient for GIRK4 was 1.4±0.1 **(Fig. 28B)**, indicating that the binding of one BD 1047 molecule to GIRK4 tetramer is sufficient to trigger the inhibition effect.

Taking advantage of the obvious differences of the effect of BD1047 on GIRK2 and GIRK4, chimeras between them were made to identify the binding site between GIRK channel and BD1047. GIRK2 was divided into five parts (N-ter, TM1, the pore forming loop between TM1 and TM2, TM2 and C-ter) and each part was replaced with that of GIRK4 **(Fig. 29A)**. In total, six chimeras, GIRK42222, GIRK24222, GIRK22422, GIRK22242, GIRK22224 and GIRK24242, were made **(Fig. 29B)**. Electrophysiological results showed that the inhibition by BD1047 on the chimeras containing the N-ter, pore forming region or C-ter of GIRK4 reaching 61.8±9.9%, 37.1±14.5% and 49.2±2.5%, respectively **(Fig. 30)**. This shows the importance of the N-ter, pore

forming region or C-ter of GIRK4 for the inhibition by BD1047. As the chimera GIRK42222 showed the strongest inhibition effect by BD1047, I decided to focus on the N-ter of GIRK4.

Another N-ter chimeras between GIRK2 and GIRK4 was constructed in which only the distal 58 amino acids out of 86 in the N-ter from GIRK4 were added to GIRK2 (GIRK2 4(1-58)2222) **(Fig. 31A)**. The results indicate that the inhibition ratio of the chimera containing the distal region of N-ter (1-58) is 20.6±1.0% which is close to that of GIRK2 WT, 12.9±5.7%, while the inhibition ratio of the chimera containing the whole N-ter is 54.1±13.4% which is close to that of GIRK4 WT, 63.6±9.5 % **(Fig. 31B)**. The results show that the distal region of N-ter of GIRK4 is not involved in the inhibition effect by BD1047 and suggest that the proximal region of N-ter (59-86) of GIRK4 is critical for the binding of BD1047.

Inhibition of GIRK2 and GIRK4 mutants by BD1047

Single point mutants on GIRK2 and GIRK4 of the proximal region of N-ter were made to identify the binding sites of BD1047. By comparing the amid acid sequence of GIRK2 and GIRK4, only three differences were found in the proximal N-ter **(Fig. 32A)**. Therefore, all these three amino acids, Arg73, Thr80 and Ile82 of GIRK2 were mutated to the corresponding amino acids of GIRK4, Gln, Ser and Leu. Only GIRK2 I82L acquired strong inhibition effect of 61.0±1.9% like GIRK4 whose inhibition percentage was 58.9±3.0% **(Fig. 32B)**. On the contrary, L77I mutant of GIRK4 was not strongly inhibited by BD1047 **(Fig. 33B)**. Taken together, it was confirmed that the position Leu77 on GIRK4 is critical for the inhibition effect of BD1047 on GIRK4 channel.

Molecular docking of GIRK4 channel and BD1047

Molecular docking is a useful approach to computationally predict the preferred binding site and docking orientation of a small molecule with a target protein. Thus, computational docking using the software named SwissDock online was conducted to approach the possible binding sites of BD1047 with GIRK4 channel. As the structure of GIRK4 has not been solved yet, a homology

structural model of GIRK4 was made based on the available structure of GIRK2 (6XIT) using SWISS-MODEL online. Then, the obtained structure of GIRK4 and the chemical structure of BD1047 were uploaded to the SwissDock site.

The computational docking result of GIRK4 and BD1047 showed that BD1047 (cyan clusters) can bind to GIRK4 channel including N-ter, pore forming region as well as C-ter **(Fig. 34)**. This result is consistent with the electrophysiological data of the GIRK2/4 chimeras **(Fig. 30)**. Besides demonstrating the possible binding positions, the docking result also predicts all the possible binding directions and orientations of BD1047 at each position. Thus, BD1047 is shown in cluster forms at each predicted binding position is due to the various directions and orientations of the binding. Therefore, when the intensity of the clusters at a position is higher, the possibility that BD1047 can bind to that position is judged to be higher. Obviously, BD1047 showed the highest intensity of the cluster at the N-ter, showing the highest chance that BD1047 interacts with GIRK4 at the N-ter **(Fig. 34)**. By highlighting the Leu77 on GIRK4 **(Fig. 34)**, it clearly demonstrates the importance of the Leu77 on GIRK4 for the binding with BD1047 which is consistent with the electrophysiological data **(Fig. 33)**.

There are some other amino acids adjacent to Leu77 in GIRK4, such as Tyr73, Leu74, Thr80, leu81 and Leu84, which might also play critical roles for the inhibition by BD1047, since it appears that they also interact with BD1047 **(Fig. 35)**. These amino acids could not be identified by comparing the sequence alignment between GIRK2 and GIRK4, because they are conserved both in GIRK2 and GIRK4 channel. I picked up some of them (Leu74, Leu81 and Leu84) and examined these point mutants. The inhibition effect of BD1047 was remarkably decreased in all of these mutants **(Fig. 36)**, conforming the validity of the computational docking results.

Discussion

The first aim of this study was to clarify whether M2R can be regulated by S1R and to identify the structural determinants. I used HEK293T cells as an in vitro expression system and observed followings: (1) By patch-clamp, it was confirmed that S1R inhibits the function of only M2R among other types of $G_{i/o}$ coupled receptors. The disease associated mutant S1R E102Q does not inhibit the function of M2R. (2) By immunohistochemical staining and confocal imaging, it was observed that the expression level of M2R on the PM is not clearly down regulated by S1R in HEK293T cells, and that of M2R on PM is slightly decreased by S1R in Hela cells. In both HEK293T and Hela cells, S1R localizes close to M2R, suggesting an interaction with M2R presumably at the ER-PM junction. (3) By co-immunoprecipitation analysis, the binding of M2R and S1R was confirmed. (4) By analyzing various chimeras and mutants of M2R and M4R, it was shown that Glu172 and Glu175 of M2R on the extracellular loop 2 region, as well as the TM6, are essential for the inhibition by S1R. Taken together, the data shows that S1R partly decreases the expression of M2R on the PM and also inhibits its function, via the extracellular loop 2 and TM6.

Furthermore, I happened to find that the BD1047, an antagonist of S1R, directly inhibits the current of GIRK channel. In order to confirm the direct inhibition of BD1047 on GIRK channels, I used Xenopus oocytes as an in vitro expression system and performed two-electrodes voltage clamp and observed followings: (1) BD1047 directly inhibits GIRK channels in the absence of S1R. (2) BD1047 has a weak inhibition effect on GIRK2 channel and a strong inhibition effect on GIRK4 channel. (3) The chimera which contains the proximal N-ter of GIRK4 showed strong inhibition effects by BD1047. Leu77 on N-ter of GIRK4 is essential for the inhibition by BD1047. (4) Molecular docking analysis showed multiple possible docking sites between GIRK4 and BD1047 and confirmed the importance of Leu77 for the binding. Taken together, the data showed that BD1047 directly inhibits GIRK channels and that GIRK4 Lue77 is essential for the inhibition by BD1047.

Regulation of M2R by S1R and its mutant S1R E102Q

Since M2R is highly expressed in cholinergic neurons in the brain (James & Cubeddu, 1987; Bernard *et al.*, 1992) and the chaperone protein S1R is also expressed throughout both the central and peripheral nervous system (Ousman *et al.*, 2017), it is possible that there might be an interaction between M2R and S1R. It was confirmed that M2R and S1R are co-localized in the postsynaptic side on the soma of motoneurons in the mouse brainstem and spinal cord (Mavlyutov *et al.*, 2010).

In the present study, I showed that S1R inhibits the function of M2R but the ALS-linked mutation, S1R E102Q, does not. An interpretation of these results may be that Glu102 of S1R is the critical interaction site with M2R, and that the interaction is lost between M2R and S1R in the E102Q mutant. However, it is also possible the E102Q mutation changes the overall structure of S1R and this position can't simply be thought as an interaction site between M2R and S1R.

It is accepted that S1R is a chaperone protein and it has multiple oligomeric forms from monomer to octamer, whereas the exact mechanisms of how it functions at the molecular level remains unclear. One reported hypothesis is that S1R functions as a chaperone protein in its lower-order oligomeric forms such as monomer and higher-order oligomers of S1R do not have a chaperone function. It was reported that S1R favors the lower-order oligomeric forms in the presence of agonists and that it stays in higher-order oligomeric forms in the presence of antagonists (Chu & Ruoho, 2016; Ryskamp *et al.*, 2019). It is also known that the S1R WT mostly exists as multimer in physiological condition and that E102Q mutation destabilizes the interaction between the bulky C-ter and the N-ter transmembrane helix, subsequently disrupting the multimerization to form such as dimers (Hong, 2020; Abramyan *et al.*, 2020). More importantly, S1R E102Q mutant loses the ligand-induced oligomerization changes, suggesting the dysfunction of S1R by E102Q mutation (Abramyan *et al.*, 2020). Thus, the interpretation for the lack of the inhibition of M2R by S1R E102Q might due to the structural disruption and loss of function in S1R.

The mechanism of the interaction between M2R and S1R

Accumulated studies illustrated the direct/indirect interaction of S1R with various proteins including ionotropic receptors (IP_3R, NMDAR), voltage-gated ion channels (K^+, Na^+, Ca^{2+}, K_{ir}), thermosensitive ion channel (TRPV1) and G-protein coupled receptors (D1R, D2R) in various subcellular compartments of the cells (Su *et al.*, 2010; Kourrich *et al.*, 2012; Smith, 2017; Ortiz-Renteria *et al.*, 2018). Although forty years have passed since S1R was first found in 1982, the molecular mechanisms how S1R regulates the function of these proteins are not clear yet.

It was reported that the interaction between TRPV1 and S1R can modulate the capsaicin-induced pain. It was showed that S1R colocalizes with TRPV1 on ER, but not on PM. Also, the protein-protein interaction between TRPV1 and S1R was demonstrated by co-immunoprecipitation study, and TM1-TM6 of TRPV1 was shown to be involved in the interaction with S1R (Ortiz-Renteria *et al.*, 2018). The results provide some evidences that TM of a PM protein is involved in the regulation by S1R, an ER membrane protein. In the present study, I showed the involvement of TM6 of M2R by chimera studies between M2R and M4R. Possible candidate amino acid residues on TM6 might be close to the intracellular side to have a better chance to interact with S1R. In addition to TM6, I also identified Glu172 and Glu175 on the extracellular loop between TM4 and TM5 as critical sites for the inhibition of M2R by S1R. Also, it was observed by IHC that M2R and S1R co-localize presumably at the ER-PM junction but not on PM. Based on these findings, it is interesting to clarify how an ER protein (S1R) affects the PM protein (M2R) through its extracellular loop and TM. Three interaction models could be proposed. They are side-by-side interaction models on PM (1) or on ER (2) and a tail-to-tail interaction model at the ER-PM junction (3) **(Fig. 37)**.

In the side-by-side model, M2R and S1R both are supposed to locate on PM (1) or on ER (2) and they interact with each other on PM or on ER. Model (1) explains the electrophysiological data that the TM6 of M2R could interact with S1R, whereas it is unclear how Glu172 and Glu175 are involved. However, the IHC data do not necessarily support this side-by-side model since it showed

that S1R is mostly expressed on ER, not on PM. Model (2) explains that the inhibition of M2R is simply due to the retention of M2R at ER, as partly supported by the IHC in Hela cells. However, the limited down regulation of the expression on PM and the strong functional inhibition in HEK293T cells cannot be fully explained by this model. In the tail-to-tail model (3) M2R locates on PM and S1R locates on ER, and they are supposed to interact with each other within the cells at the ER-PM junction. This model can go well with the IHC data that M2R and S1R are located in the proximity to colocalize together, presumably at the ER-PM junction. However, tail-to-tail model cannot explain how Glu172 and Glu175 on the extracellular loop are involved in the interaction, although the involvement of the interaction of TM6 could be explained if the site is at the beginning of TM6 close to the cytoplasmic side. One possible explanation for the involvement of Glu172 and Glu175 is that Glu172 and Glu175 are allosteric sites of M2R (May *et al.*, 2007), and that mutation at these positions might result in the conformational change of M2R. It will lead to the change of other interaction site(s) on M2R, which results in the loss of the interaction between M2R and S1R.

Although it is still hard to combine all data to draw a straightforward conclusion about the entire mechanism of the interaction between M2R and S1R, it was explicitly identified that the Glu172, Glu175 in the extracellular loop and TM6 of M2R are critical sites for the inhibition by S1R.

The effect of BD1047 on S1R and GIRK channel

BD1047 is classified as one of the antagonists of S1R. The application of BD1047 potentiates S1R transforming from monomer or dimer form into tetramer form which loses the chaperone function (Chu & Ruoho, 2016; Ryskamp *et al.*, 2019). It is known that process of the assembling and transforming from one oligomeric state to another such as from monomer to tetramer could not be occurred in a short time scale. However, the application of BD1047 to the oocyte immediately produced an effective inhibition on GIRK channel within 5 seconds, a very short time course. This

indicates that even in the presence of S1R, the inhibition effects of BD1047 may be due to the direct inhibition on GIRK current, but not due to the block of the function of S1R via changing its oligomeric state by BD1047. Therefore, both in the presence or absence of S1R coexpression, the rapid decrease in the GIRK current by BD1047 is more likely caused by the direct inhibition on GIRK channel.

Binding sites of BD1047 to GIRK4 and computational docking results

Leu77 in the proximal N-ter cytoplasmic region of GIRK4 was identified as a critical site for the inhibition effect of BD1047 and the importance of Leu77 for the direct binding of BD1047 to GIRK4 was confirmed by molecular docking study.

It also raised candidates of other critical amino acid residues adjacent to Leu77, i.e. Leu74, Leu81 and Leu 84 conserved in GIRK2 and GIRK4, which were confirmed to be functionally critical for the inhibition by BD1047. Thus, it was shown that computational docking data indeed help the confirmation of the incomplete mutagenesis study and provides quite comprehensive and accurate information. However, as its trustability is not necessarily guaranteed, the combined usage with electrophysiological analysis of chimeras and mutants performed in this study is indispensable to draw a solid conclusion.

The mechanism of the binding between BD1047 and GIRK4 channel

In the mutagenesis studies revealing the structural determinants for the inhibition of GIRK4 channel by BD1047, the inhibition ratio of BD1047 on GIRK4 L77I was partly decreased compared to that of GIRK4 WT, but it did not reach down to the same level as GIRK2 WT.

One possibility is that there might be other region(s) on GIRK4 which contribute to the binding with BD1047. GIRK2/4 chimera studies also showed a possible involvement of the pore forming region and the C-ter of GIRK4, which are consistent with the results of the molecular docking study.

Another possibility for the partly loss of inhibition is that it is due to a rather limited effect of the conservative mutation effect of L77I, in which hydrophobicity is maintained. BD1047 could pass through the lipid bilayer membrane of oocyte to bind with the N-ter of GIRK4 that is located in the cytosolic side, suggesting that BD1047 possesses hydrophobicity. On the other hand, Leu77 as well as Leu74, Leu81 and Leu84 also has hydrophobicity which will enable a hydrophobic interaction with BD1047. In the electrophysiological analysis, the inhibition of GIRK4 by BD1047 was completely lost when either Leu74, Leu81 or Leu84 was mutated to alanine, whereas inhibition by BD1047 was only partly attenuated by L77I mutation. These results suggest that the hydrophobicity of the amino acid residue may be critical for the binding between BD1047 and GIRK4 channel.

The Leu77 on GIRK4 may be a common drug binding site

Our group reported previously that the antiparasitic drug, ivermectin (IVM), can activate GIRK channels and the critical amino acid residue for the activation of the GIRK2 by IVM is Ile82. Ile82 is located in the slide helix between the TM1 and the N-terminal cytoplasmic tail domain (CTD) (Chen *et al.*, 2017). In my experiments, Leu77 of GIRK4, correspondingly to Ile82 of GIRK2, was identified as the critical amino acid residue for the inhibition effect by BD1047. Since both IVM and BD1047 bind to the slide helix region, it would be interesting to see whether the binding of one ligand could affect the binding of the other. For instance, whether BD1047 still has a strong inhibition effect on GIRK4 activated by IVM. Furthermore, other groups showed the role GIRK4 Leu77 (corresponding to GIRK2 Ile82) in the activation by a novel activator 3hi2one-G4 (Cui *et al.*, 2022). Taken together, both activators and an inhibitor which have different structure bind to this slide helix region between TM1 and CTD of GIRK channel, suggesting that this position might be a shared hot spot for the drug binding, which could be used as therapeutic target to develop new medicines for GIRK channel-associated diseases.

References

Abramyan AM, Yano H, Xu M, Liu L, Naing S, Fant AD & Shi L. (2020). The Glu102 mutation disrupts higher-order oligomerization of the sigma 1 receptor. *Comput Struct Biotechnol J* **18,** 199-206.

Aydar E, Palmer CP, Klyachko VA & Jackson MB. (2002). The sigma receptor as a ligand-regulated auxiliary potassium channel subunit. *Neuron* **34,** 399-410.

Bernard V, Normand E & Bloch B. (1992). Phenotypical characterization of the rat striatal neurons expressing muscarinic receptor genes. *J Neurosci* **12,** 3591-3600.

Chen IS, Tateyama M, Fukata Y, Uesugi M & Kubo Y. (2017). Ivermectin activates GIRK channels in a PIP(2) -dependent, G(betagamma) -independent manner and an amino acid residue at the slide helix governs the activation. *J Physiol* **595,** 5895-5912.

Chu UB & Ruoho AE. (2016). Biochemical Pharmacology of the Sigma-1 Receptor. *Mol Pharmacol* **89,** 142-153.

Cui M, Xu K, Gada KD, Shalomov B, Ban M, Eptaminitaki GC, Kawano T, Plant LD, Dascal N & Logothetis DE. (2022). A novel small-molecule selective activator of homomeric GIRK4 channels. *J Biol Chem* **298,** 102009.

Dreser A, Vollrath JT, Sechi A, Johann S, Roos A, Yamoah A, Katona I, Bohlega S, Wiemuth D, Tian Y, Schmidt A, Vervoorts J, Dohmen M, Beyer C, Anink J, Aronica E, Troost D, Weis J & Goswami A. (2017). The ALS-linked E102Q mutation in Sigma receptor-1 leads to ER stress-mediated defects in protein homeostasis and dysregulation of RNA-binding proteins. *Cell Death Differ* **24,** 1655-1671.

Fontanilla D, Hajipour AR, Pal A, Chu UB, Arbabian M & Ruoho AE. (2008). Probing the steroid binding domain-like I (SBDLI) of the sigma-1 receptor binding site using N-substituted photoaffinity labels. *Biochemistry* **47,** 7205-7217.

Fredriksson R, Lagerstrom MC, Lundin LG & Schioth HB. (2003). The G-protein-coupled receptors in the human genome form five main families. Phylogenetic analysis, paralogon groups, and fingerprints. *Mol Pharmacol* **63,** 1256-1272.

Gromek KA, Suchy FP, Meddaugh HR, Wrobel RL, LaPointe LM, Chu UB, Primm JG, Ruoho AE, Senes A & Fox BG. (2014). The oligomeric states of the purified sigma-1 receptor are stabilized by ligands. *J Biol Chem* **289,** 20333-20344.

Hayashi T & Su TP. (2003). Intracellular dynamics of sigma-1 receptors (sigma(1) binding sites) in NG108-15 cells. *The Journal of pharmacology and experimental therapeutics* **306,** 726-733.

Hayashi T & Su TP. (2007). Sigma-1 receptor chaperones at the ER-mitochondrion interface regulate Ca(2+) signaling and cell survival. *Cell* **131,** 596-610.

Hibino H, Inanobe A, Furutani K, Murakami S, Findlay I & Kurachi Y. (2010). Inwardly rectifying potassium channels: their structure, function, and physiological roles. *Physiological reviews* **90,** 291-366.

Hong WC. (2020). Distinct Regulation of sigma (1) Receptor Multimerization by Its Agonists and Antagonists in Transfected Cells and Rat Liver Membranes. *The Journal of pharmacology and experimental therapeutics* **373,** 290-301.

James MK & Cubeddu LX. (1987). Pharmacologic characterization and functional role of muscarinic autoreceptors in the rabbit striatum. *The Journal of pharmacology and experimental therapeutics* **240,** 203-215.

Kourrich S, Su TP, Fujimoto M & Bonci A. (2012). The sigma-1 receptor: roles in neuronal plasticity and disease. *Trends Neurosci* **35,** 762-771.

Logothetis DE, Kurachi Y, Galper J, Neer EJ & Clapham DE. (1987). The beta gamma subunits of GTP-binding proteins activate the muscarinic K+ channel in heart. *Nature* **325,** 321-326.

Mavlyutov TA, Epstein ML, Andersen KA, Ziskind-Conhaim L & Ruoho AE. (2010). The sigma-1 receptor is enriched in postsynaptic sites of C-terminals in mouse motoneurons. An anatomical and behavioral study. *Neuroscience* **167,** 247-255.

Mavlyutov TA & Ruoho AE. (2007). Ligand-dependent localization and intracellular stability of sigma-1 receptors in CHO-K1 cells. *Journal of molecular signaling* **2,** 8.

May LT, Avlani VA, Langmead CJ, Herdon HJ, Wood MD, Sexton PM & Christopoulos A. (2007). Structure-function studies of allosteric agonism at M2 muscarinic acetylcholine receptors. *Mol Pharmacol* **72,** 463-476.

Mishra AK, Mavlyutov T, Singh DR, Biener G, Yang J, Oliver JA, Ruoho A & Raicu V. (2015). The sigma-1 receptors are present in monomeric and oligomeric forms in living cells in the presence and absence of ligands. *The Biochemical journal* **466,** 263-271.

Mistry R, Dowling MR & Challiss RA. (2005). An investigation of whether agonist-selective receptor conformations occur with respect to M2 and M4 muscarinic acetylcholine receptor signalling via Gi/o and Gs proteins. *Br J Pharmacol* **144,** 566-575.

Ortega-Roldan JL, Ossa F, Amin NT & Schnell JR. (2015). Solution NMR studies reveal the location of the second transmembrane domain of the human sigma-1 receptor. *FEBS letters* **589,** 659-665.

Ortega-Roldan JL, Ossa F & Schnell JR. (2013). Characterization of the human sigma-1 receptor chaperone domain structure and binding immunoglobulin protein (BiP) interactions. *J Biol Chem* **288,** 21448-21457.

Ortiz-Renteria M, Juarez-Contreras R, Gonzalez-Ramirez R, Islas LD, Sierra-Ramirez F, Llorente I, Simon SA, Hiriart M, Rosenbaum T & Morales-Lazaro SL. (2018). TRPV1 channels and

the progesterone receptor Sig-1R interact to regulate pain. *Proc Natl Acad Sci U S A* **115,** E1657-E1666.

Ousman SS, Frederick A & Lim EF. (2017). Chaperone Proteins in the Central Nervous System and Peripheral Nervous System after Nerve Injury. *Frontiers in neuroscience* **11,** 79.

Pal A, Hajipour AR, Fontanilla D, Ramachandran S, Chu UB, Mavlyutov T & Ruoho AE. (2007). Identification of regions of the sigma-1 receptor ligand binding site using a novel photoprobe. *Mol Pharmacol* **72,** 921-933.

Ryskamp DA, Korban S, Zhemkov V, Kraskovskaya N & Bezprozvanny I. (2019). Neuronal Sigma-1 Receptors: Signaling Functions and Protective Roles in Neurodegenerative Diseases. *Frontiers in neuroscience* **13,** 862.

Sabeti J, Nelson TE, Purdy RH & Gruol DL. (2007). Steroid pregnenolone sulfate enhances NMDA-receptor-independent long-term potentiation at hippocampal CA1 synapses: role for L-type calcium channels and sigma-receptors. *Hippocampus* **17,** 349-369.

Schmidt HR, Zheng S, Gurpinar E, Koehl A, Manglik A & Kruse AC. (2016). Crystal structure of the human sigma1 receptor. *Nature* **532,** 527-530.

Smith SB. (2017). Introduction to Sigma Receptors: Their Role in Disease and as Therapeutic Targets. *Adv Exp Med Biol* **964,** 1-4.

Su TP, Hayashi T, Maurice T, Buch S & Ruoho AE. (2010). The sigma-1 receptor chaperone as an inter-organelle signaling modulator. *Trends Pharmacol Sci* **31,** 557-566.

Su TP, Su TC, Nakamura Y & Tsai SY. (2016). The Sigma-1 Receptor as a Pluripotent Modulator in Living Systems. *Trends Pharmacol Sci* **37,** 262-278.

Wickman K & Clapham DE. (1995). Ion channel regulation by G proteins. *Physiological reviews* **75,** 865-885.

Figures

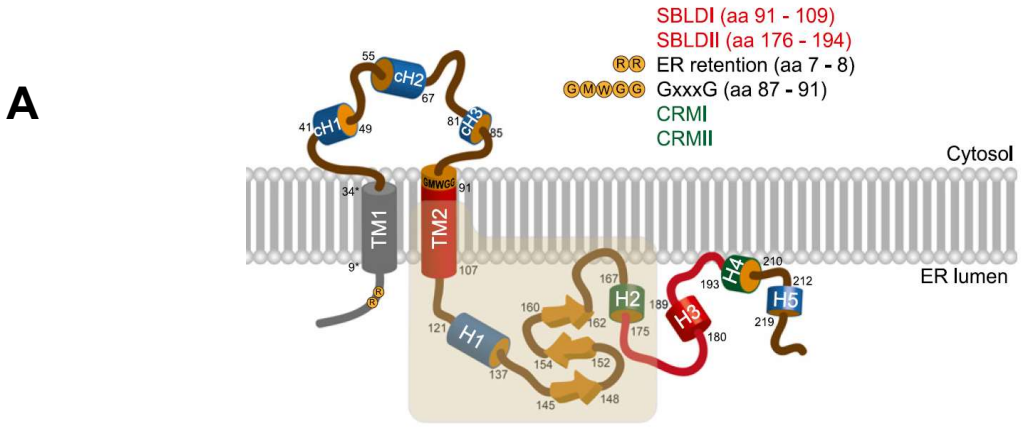

(cited from Fig. 3A of Chu & Ruoho, 2016)

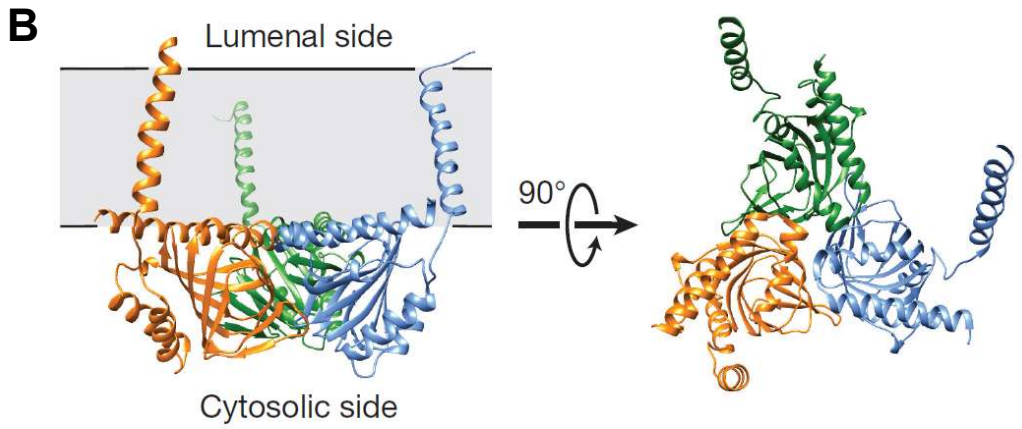

(cited from Fig. 1a of Schmidt *et al.*, 2016)

Fig. 1 Overall structure and topology of the S1R

(A) A two-TMs model of the S1R. The structure was determined by solution NMR studies. The model of the S1R is drawn from the perspectives of the ER membrane with the N and C termini at the luminal side (Chu & Ruoho, 2016). (B) The crystalized S1R showed a triangular structure comprised of three associated protomers, each with a single TM. The ER membrane plane is indicated in grey. The small N-ter of S1R is in the luminal side and the bulky C-ter is in the cytosolic side (Schmidt *et al.*, 2016).

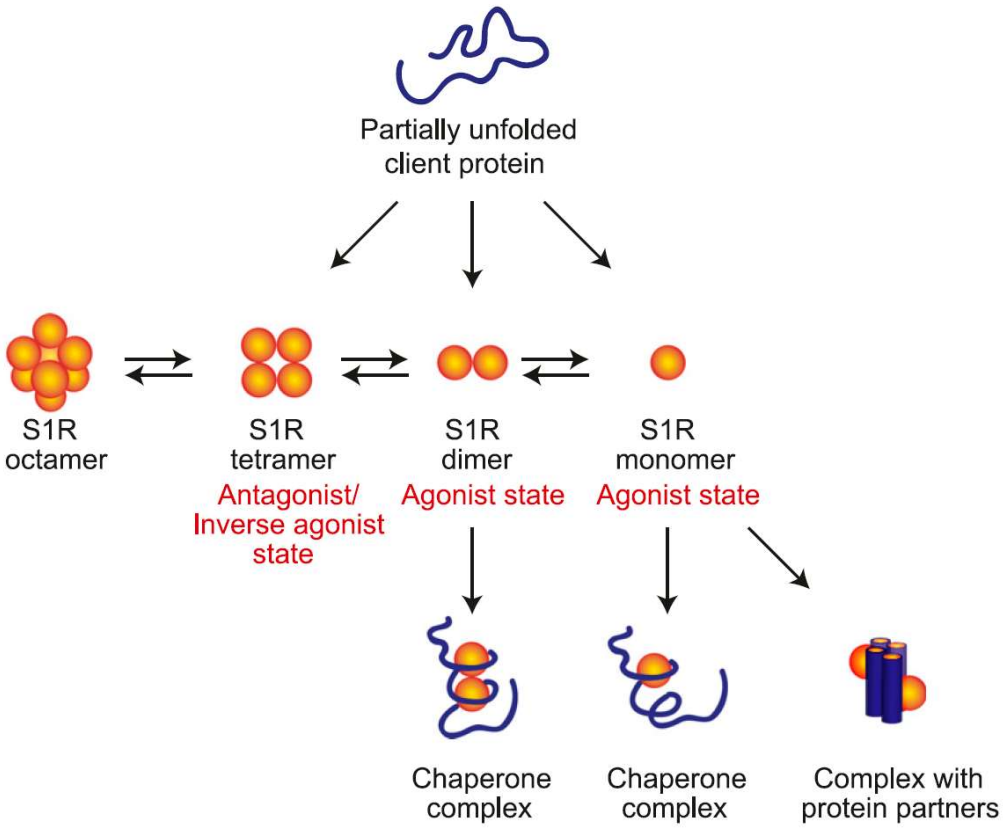

(cited from Fig. 4 of Chu & Ruoho, 2016)

Fig. 2 Proposed models of the S1R oligomerization-state-dependent function

(A) S1R is reported to show various oligomeric forms from monomer to octamer in vivo. Lower-order oligomers of S1R function as chaperone protein, but higher-order oligomers do not have chaperone function. Agonist-bound S1R favors lower-order forms such as monomer and dimer and the application of antagonists of S1R induces a shift to higher-order forms such as tetramers (Chu & Ruoho, 2016).

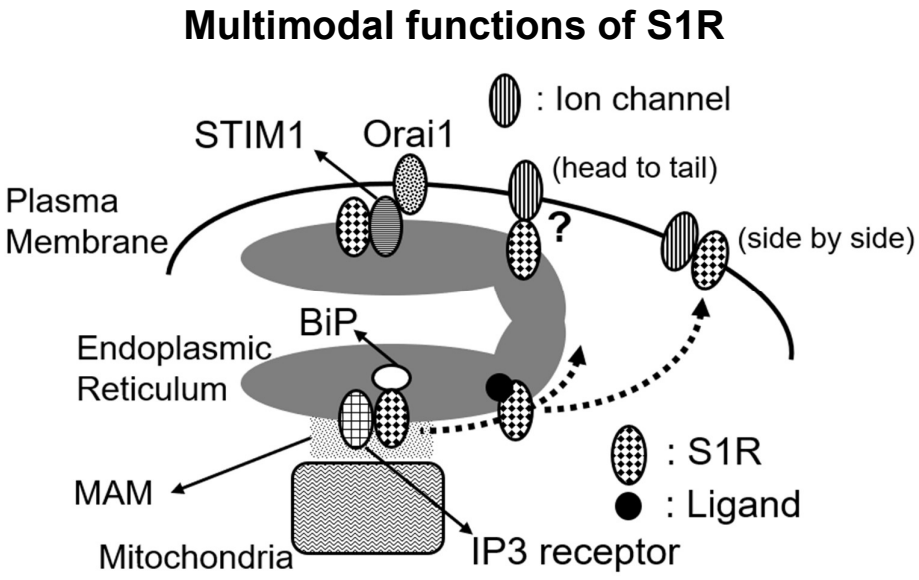

Fig. 3 Multimodal functions of S1R

S1R is known as an ER-resident protein which is chiefly located in the MAM region and it has been reported to directly/ indirectly interact with ion channels such as K_v, Na_v or K_{ir} channels. Its agonist could induce the re-distribution of S1R from MAM to the PM (side-by-side) or to the ER-PM junction (head-to-tail) and subsequently induce effects on various ion channels. The dashed lines represent possible trafficking pathways of S1R from ER to PM upon its ligand binding.

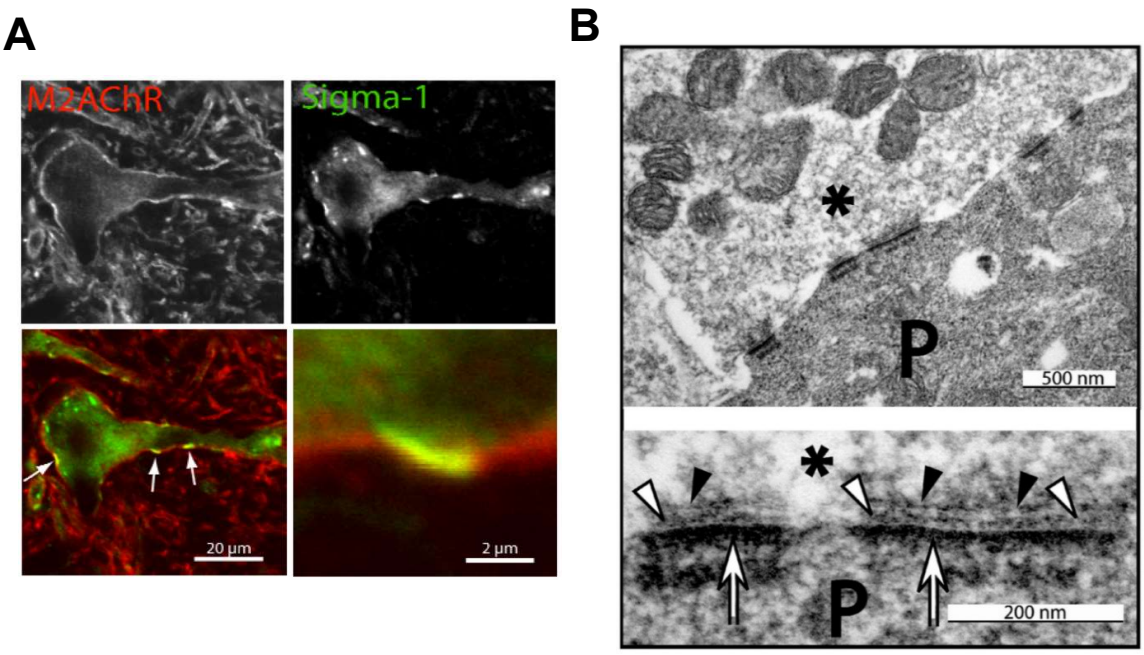

(cited from Fig. 3A of Mavlyutov *et al.*, 2010) (cited from Fig. 4 of Mavlyutov *et al.*, 2010)

Fig. 4 Colocalization of M2R and S1R at the postsynaptic site of motoneurons

(A) IHC results showed that S1R is colocalized with M2R receptor at the postsynaptic site of motoneurons in the ventral horn of mouse, indicated by white arrows (Mavlyutov *et al.*, 2010). (B) Ultrastructural localization of S1R. (Top panel) Electron-dense precipitate appears on the postsynaptic side close to the PM. (Bottom panel) Higher magnification of the synaptic contact. The dense signal appears separated from the PM and is likely to be at the subsurface ER cisternae, indicating the S1R signal is located close but apart from the PM. Asterisk indicates the presynaptic side; P indicates the postsynaptic side; Black arrowheads point to the presynaptic membrane; open arrowheads point to the postsynaptic membrane; arrows point to S1R (Mavlyutov *et al.*, 2010).

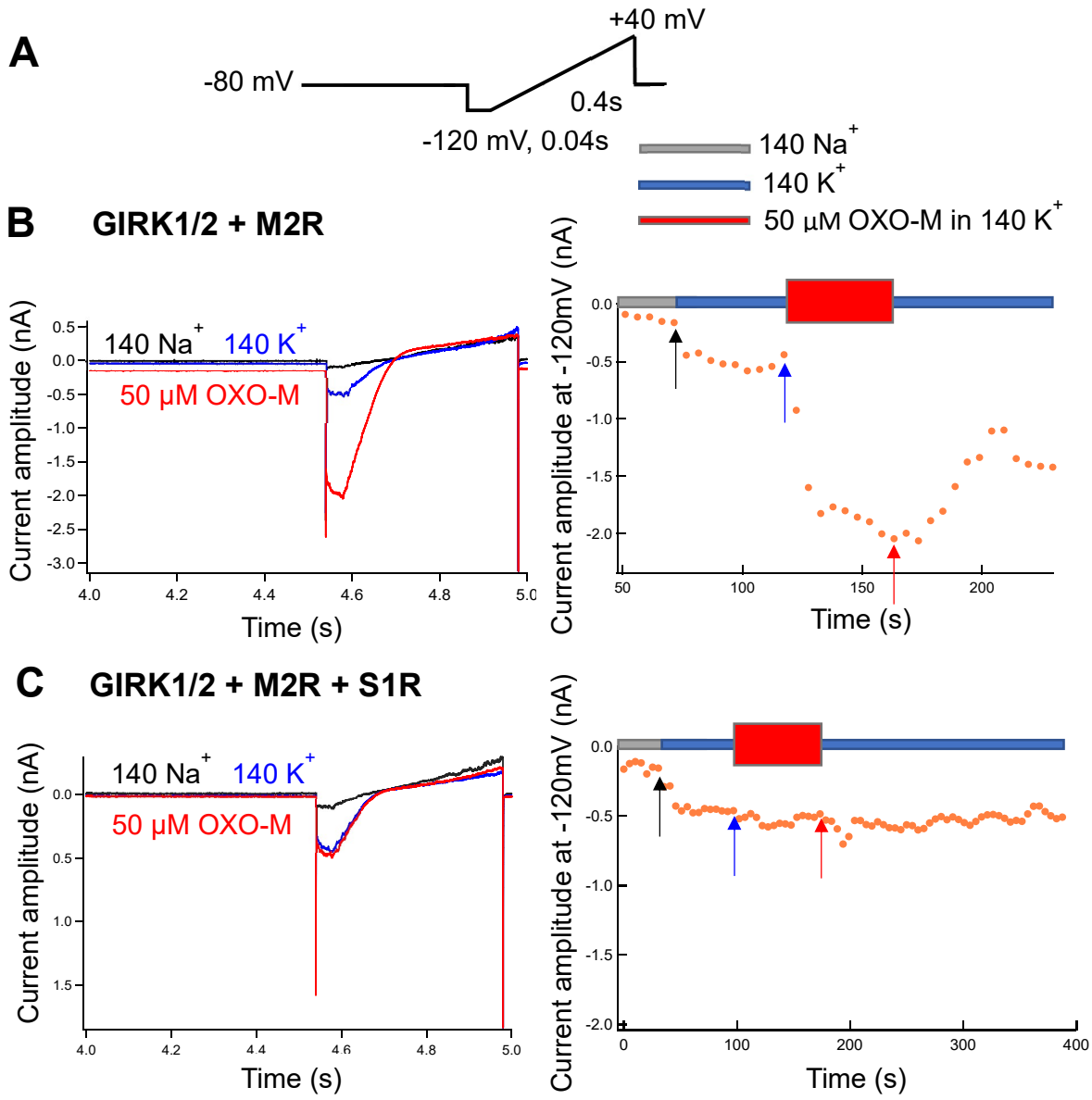

Fig. 5 The regulation of M2R by S1R measured by GIRK1/2 current

(A) A voltage ramp pulse protocol used in whole cell patch-clamp recording. Holding potential was at -80mV, and a short step to -120mV for 0.04 s and then a ramp pulse from -120mV to +40 mV within 0.4s were applied. The pulses were applied every 2 sec. (B) Recordings from HEK293T cells transfected with GIRK1/2 and M2R. (C) Recordings from HEK293T cells transfected with GIRK1/2, M2R and S1R. Left panels in (B) and (C): Representative current traces evoked by ramp pulses in 140Na^+ (Black), 140K^+ (Blue) and 140K^+ with 50µM OXO-M (Red), respectively. Right panels in (B) and (C): Timelapse changes of the current amplitude at -120mV in different bath solutions. Black, blue and red arrows indicate the time points of representative current traces shown in the left panel in 140Na^+, 140K^+ and 140K^+ with 50µM OXO-M, respectively.

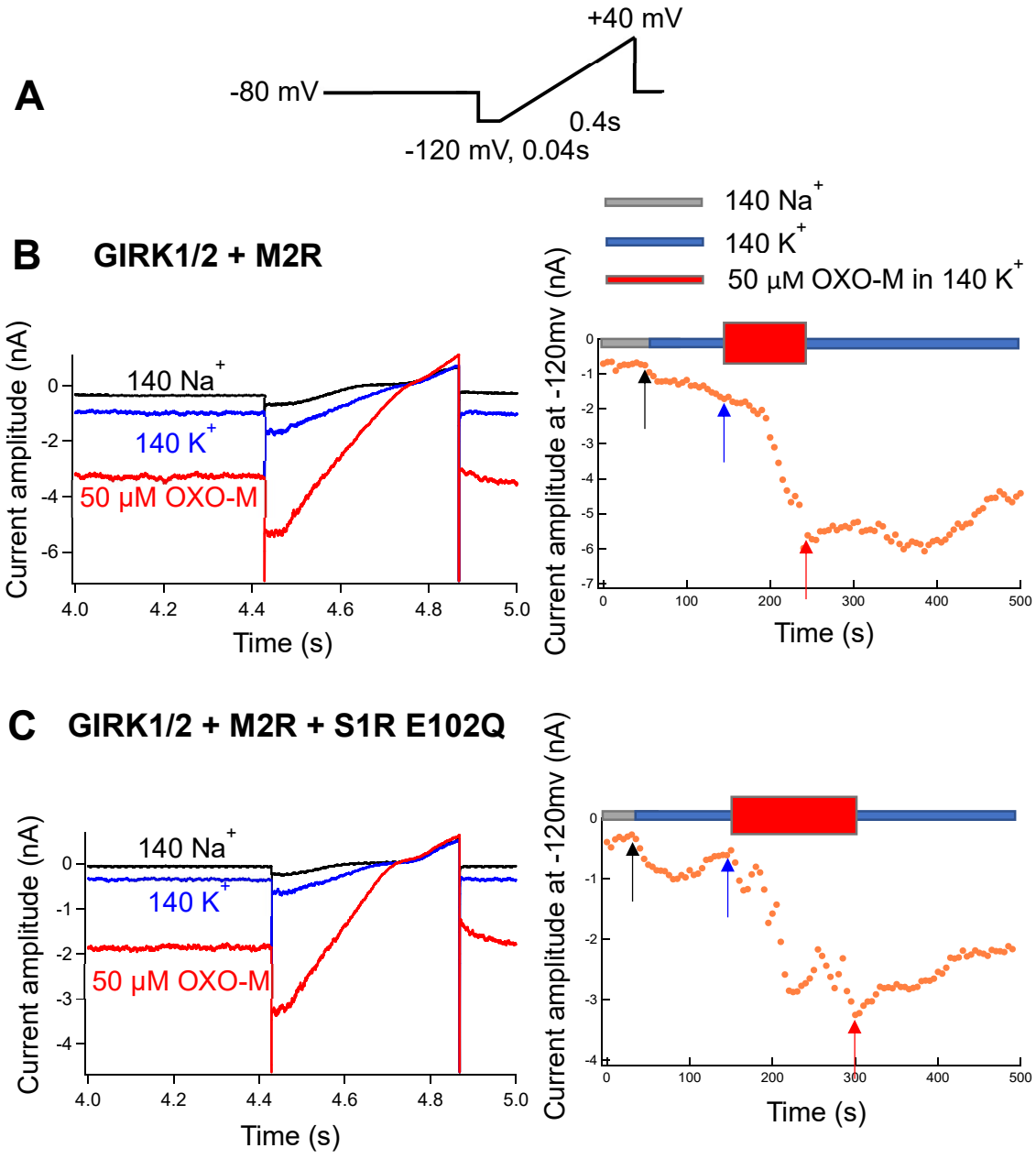

Fig. 6 The regulation of M2R by S1R E102Q measured by GIRK1/2 current

(A) A voltage ramp pulse protocol used in whole cell patch-clamp recording. (B) Recordings from HEK293T cells transfected with GIRK1/2 and M2R. (C) Recordings from HEK293T cells transfected with GIRK1/2, M2R and S1R E102Q. Left panels in (B) and (C): Representative current traces evoked by ramp pulses in $140Na^+$ (Black), $140K^+$ (Blue) and $140K^+$ with 50µM OXO-M (Red), respectively. Right panels in (B) and (C): Timelapse change of the current amplitude at -120mV in different bath solutions. Black, blue and red arrows indicate the time points of representative current traces shown in the left panel in $140Na^+$, $140K^+$ and $140K^+$ with 50µM OXO-M, respectively.

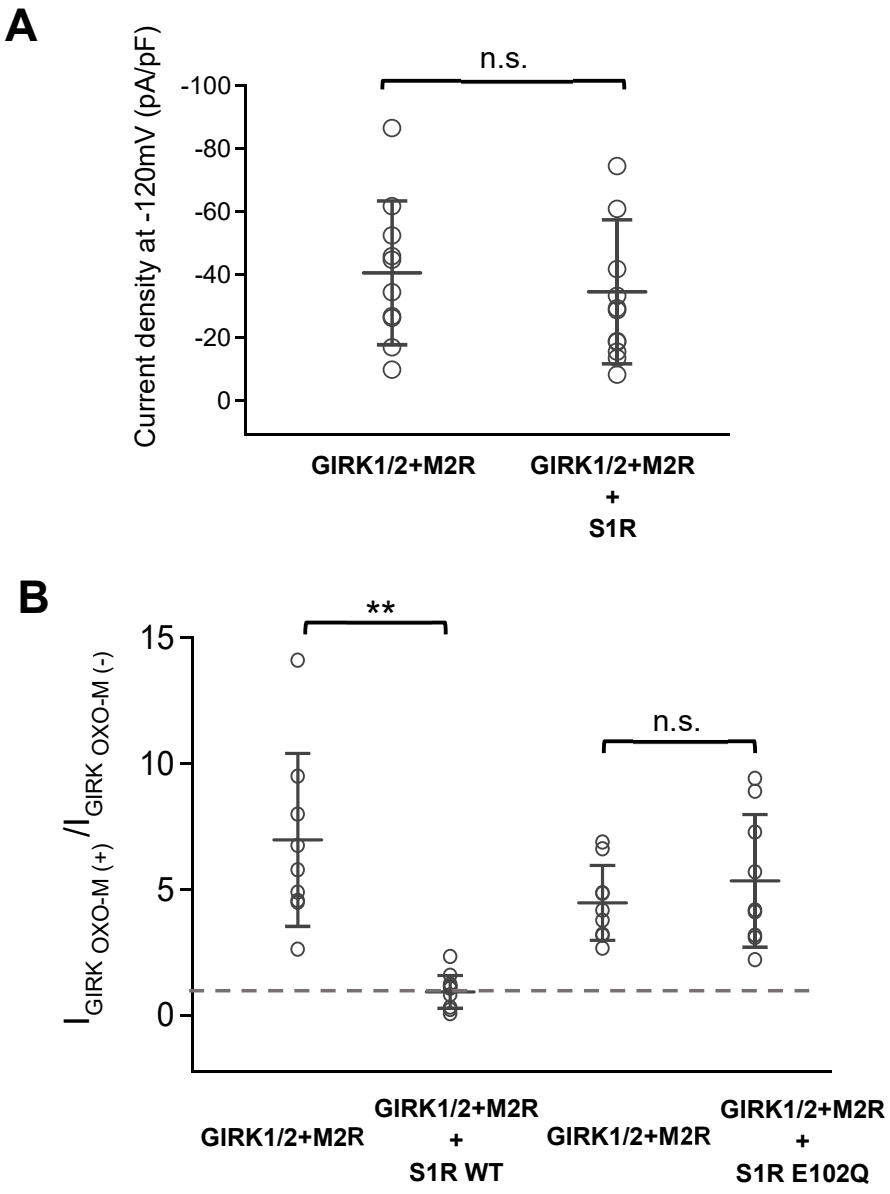

Fig. 7 The regulation of M2R by S1R and S1R E102Q measured by GIRK1/2 current

(A) Comparison of basal GIRK1/2 current densities in GIRK1/2 and M2R transfected HEK293T cells (left) or GIRK1/2, M2R and S1R transfected cells (right). Data are mean ± SD (n =10,12). Unpaired Student's *t*-test, n.s. indicates no statically significant difference. (B) Comparison of the ratio of the GIRK1/2 current before and after application of OXO-M in GIRK1/2+M2R, GIRK1/2+M2R+S1R, GIRK1/2+M2R, GIRK1/2+M2R+S1R E102Q transfected cells. Data are mean ± SD (n=9, 11, 9, 9). Student's *t*-test (Unpaired), ** indicates $P<0.01$, n.s. indicates no statically significant difference.

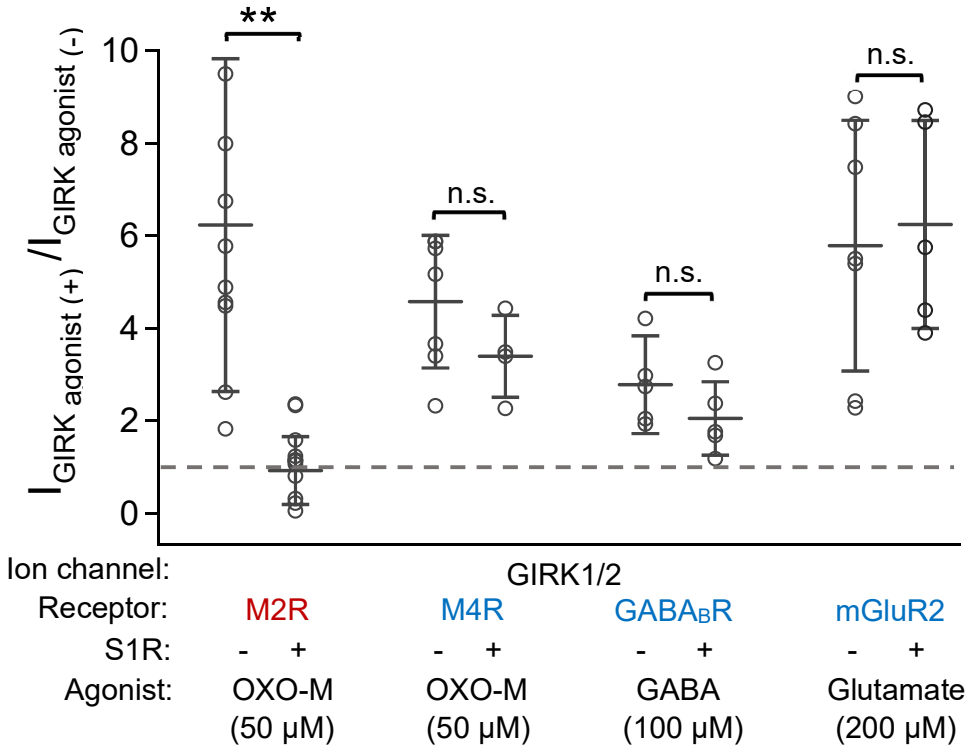

Fig. 8 The regulation of various $G_{i/o}$ coupled receptors by S1R measured by GIRK1/2 current

Comparison of the ratio of the GIRK1/2 current before and after application of their own agonists in GIRK1/2+M2R, GIRK1/2+M4R, GIRK1/2+$GABA_BR$ and GIRK1/2+ mGluR2 without or with S1R co-transfected cells. Data are mean ± SD (n=6-12). Student's *t*-test 9 (Unpaired), ** indicates $P<0.01$.

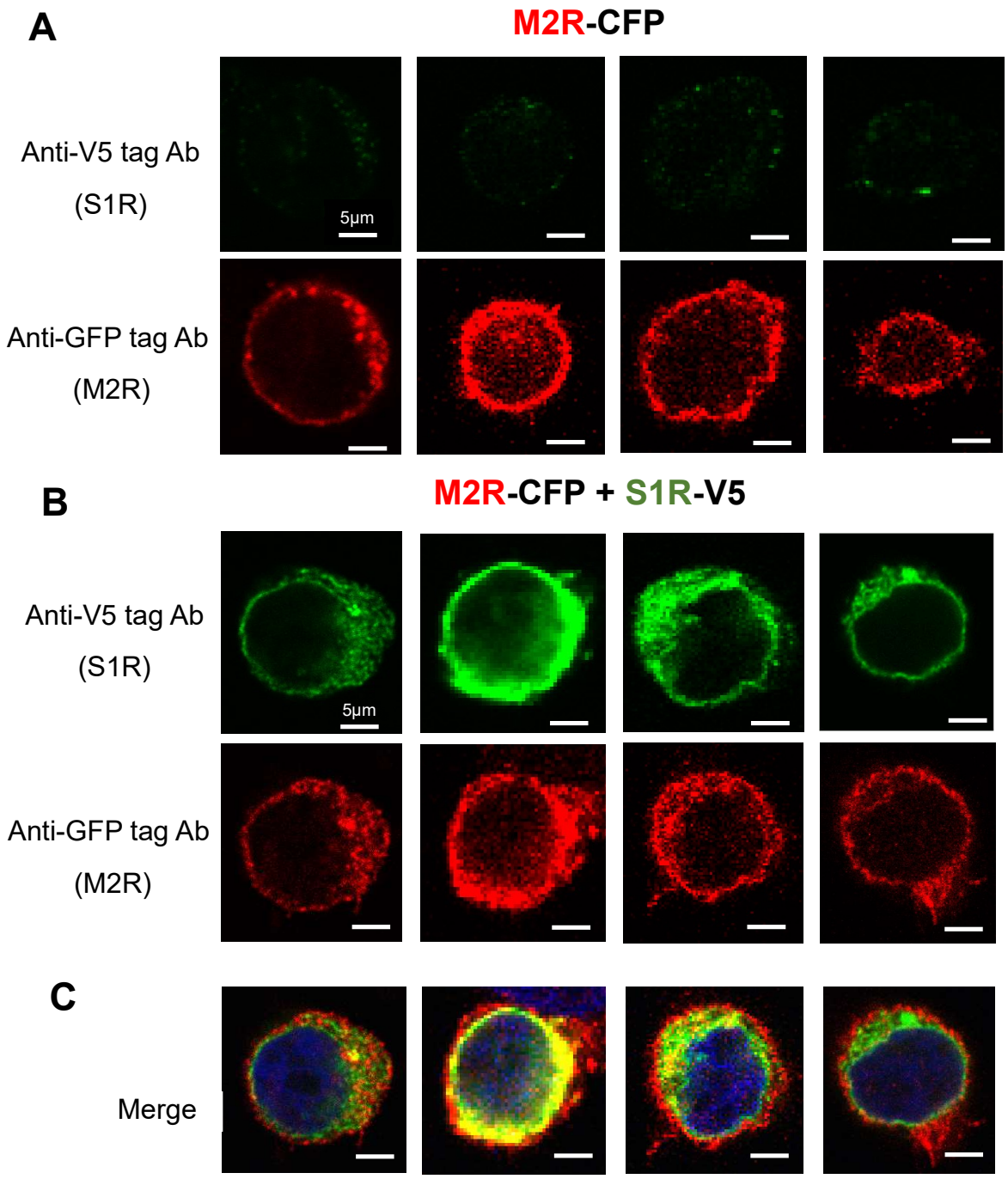

Fig. 9 Immunohistochemical staining of S1R and M2R in HEK293T cells

(A) HEK293T cells were transfected with only M2R-CFP. (B) HEK were co-transfected with M2R-CFP and S1R-V5. (C) Merged images of M2R with S1R showing the co-localization of these two proteins in yellow. M2R is detected by GFP antibody indicated in red, S1R is detected by V5 antibody indicated in green, nucleus is indicated in blue. Scale bar, 5 μm. All images were observed under confocal microscope.

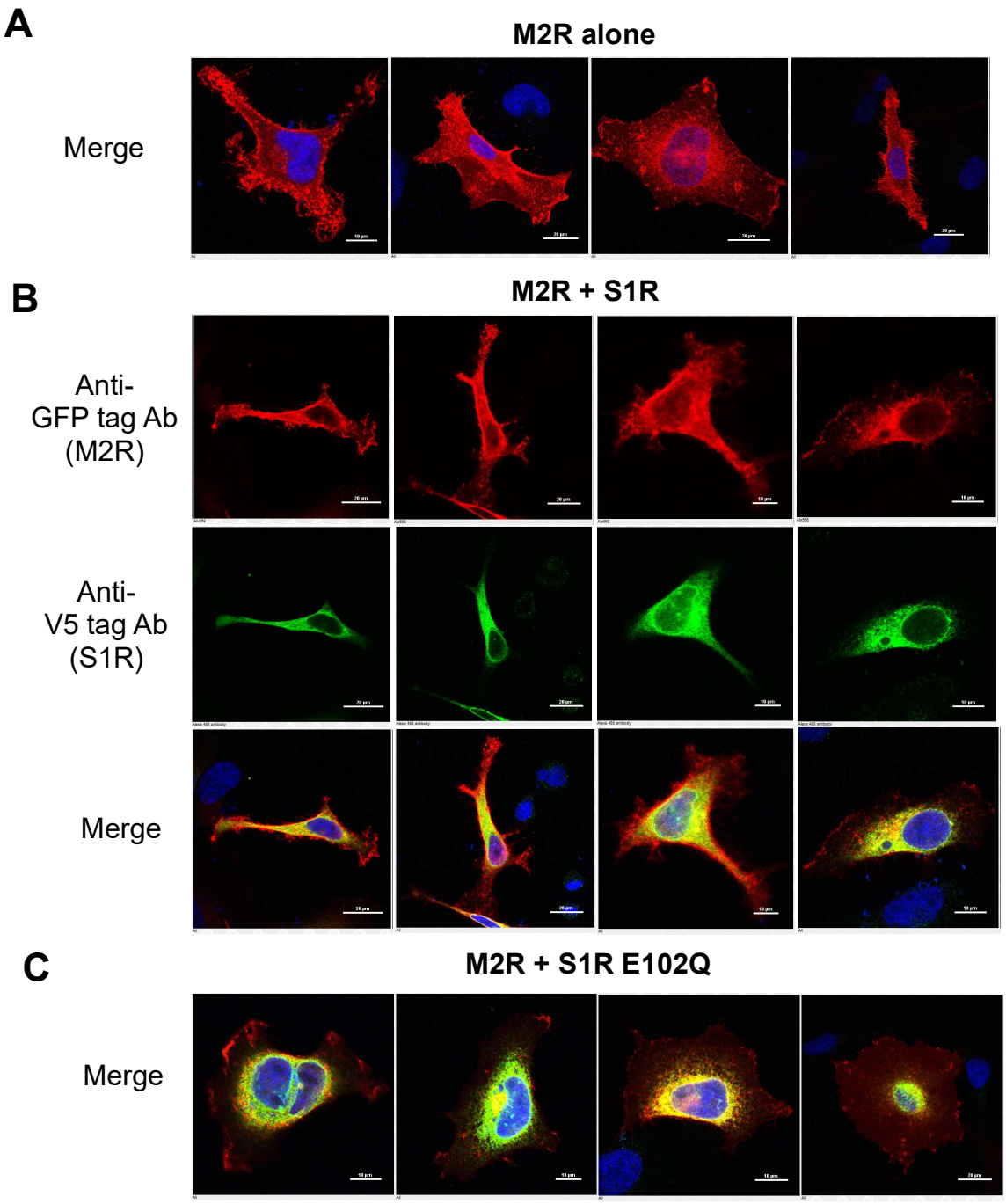

Fig. 10 Immunohistochemical staining of M2R with S1R or S1R E102Q in Hela cells

Hela cells were transfected with M2R alone (A), M2R and S1R (B), M2R and S1R E102Q (C). S1R is indicated in green, M2R is indicated in red. Merged images of S1R with M2R showing the co-localization of S1R and M2R in yellow. Nucleus is indicated in blue. Scale bar, 20 μm. All images were observed under confocal microscope.

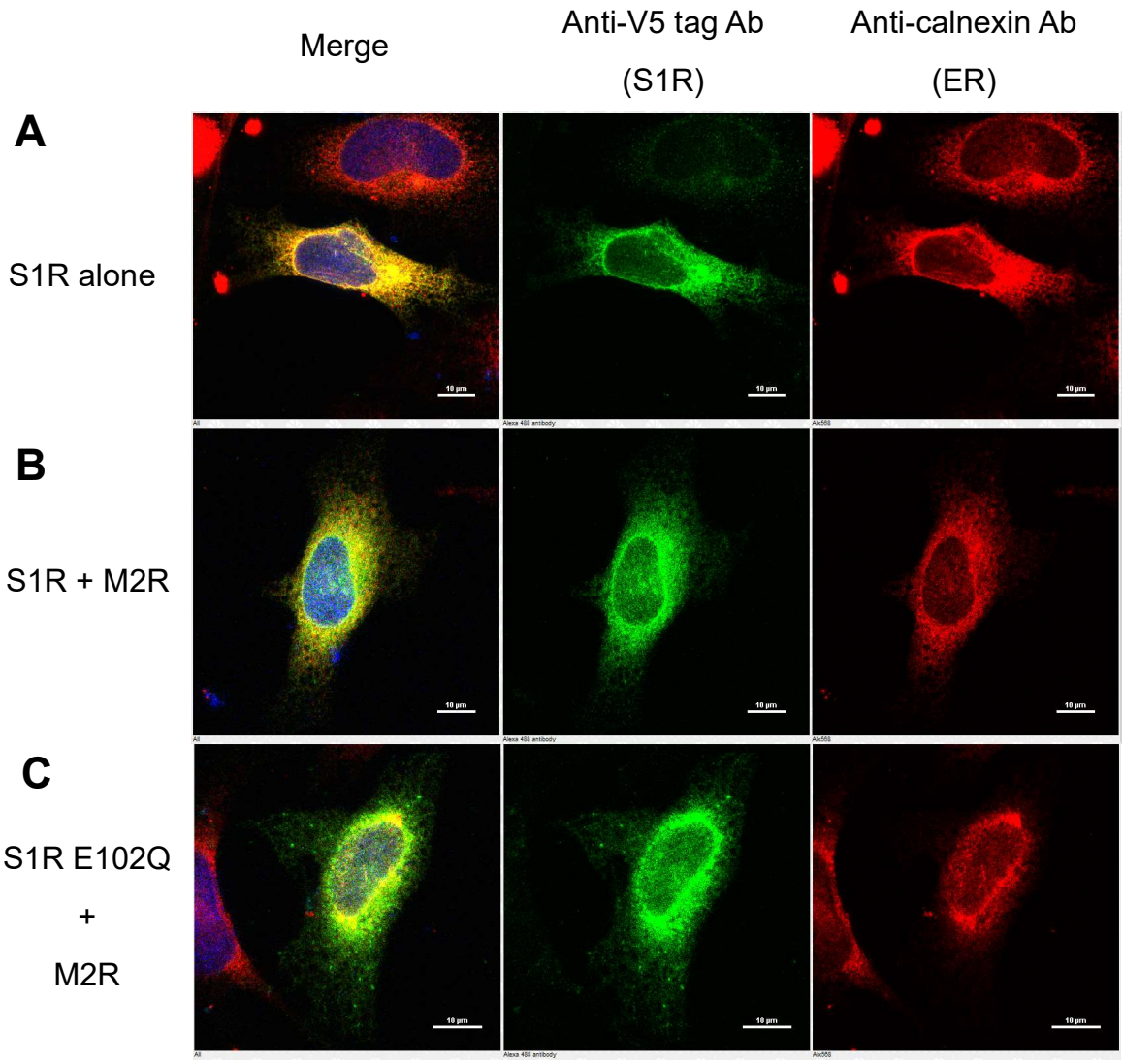

Fig. 11 Immunohistochemical staining of S1R and ER in Hela cells

Hela cells were transfected with S1R alone (A), M2R and S1R (B), M2R and S1R E102Q (C). S1R is indicated in green, ER marker protein calnexin is indicated in red. Merged images of S1R with calnexin showing the co-localization of S1R and ER in yellow. Nucleus is indicated in blue. Scale bar, 10 μm. All images were observed under confocal microscope.

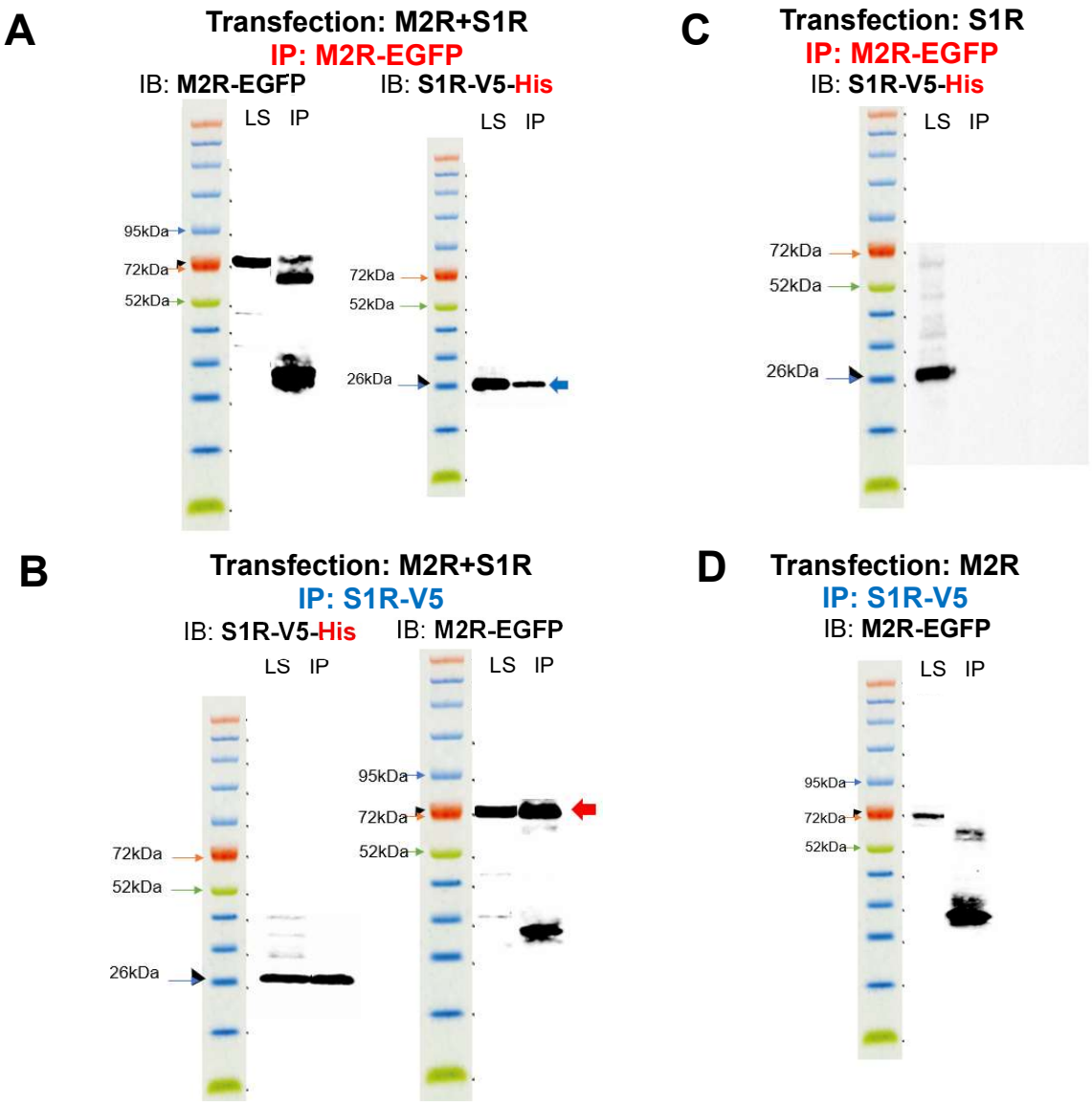

Fig. 12 Co-immunoprecipitation of M2R-EGFP and S1R-V5-His in HEK293T cells

(A) S1R co-precipitated with M2R. Left panel: M2R was precipitated by anti-EGFP tag mouse antibody and detected by anti-M2R rabbit antibody. Cell lysate sample (LS) and IP sample (IP) shows the presence of M2R. Right panel: S1R was detected by anti-His tag rabbit antibody. LS shows the expression of S1R and IP shows S1R co-precipitated with M2R (blue arrow). (C) Negative control experiments using cells transfected only with S1R and precipitated by anti-EGFP mouse tag antibody (for M2R precipitation). (B) M2R co-precipitated with S1R. Left panel: S1R was precipitated by anti-V5 tag mouse antibody and detected by anti-His tag rabbit antibody. LS and IP sample shows the presence of S1R. Middle panel: M2R was detected by anti-M2R rabbit antibody. LS shows the expression of M2R and IP sample shows M2R co-precipitated with S1R (red arrow). (D) Negative control experiments using cells transfected only with M2R and precipitated by anti-V5 mouse tag antibody (for S1R precipitation).

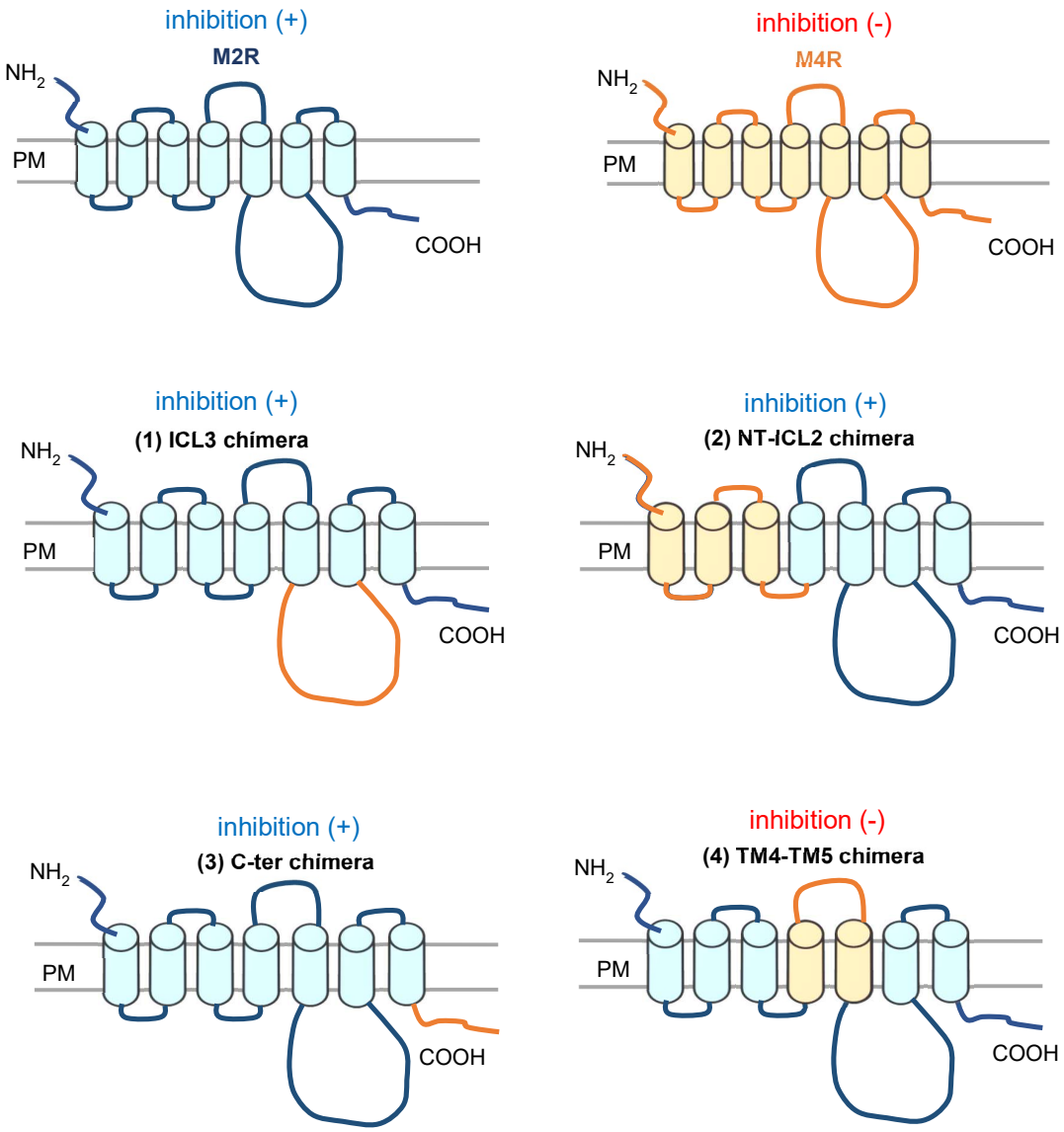

Fig. 13 Schematic drawings of chimeras between M2R and M4R

(Top panel) A topological model of M2R WT is indicated in blue and that of M4R WT is indicated in yellow. Bule and yellow columns embedded in PM indicate TMs from TM1 to TM7 of M2R and M4R respectively. (Middle and bottom panel) Chimeras of M2R (blue) in which M4R segments (yellow) of ICL3, NT-ICL2, C-ter and TM4-TM5 were introduced.

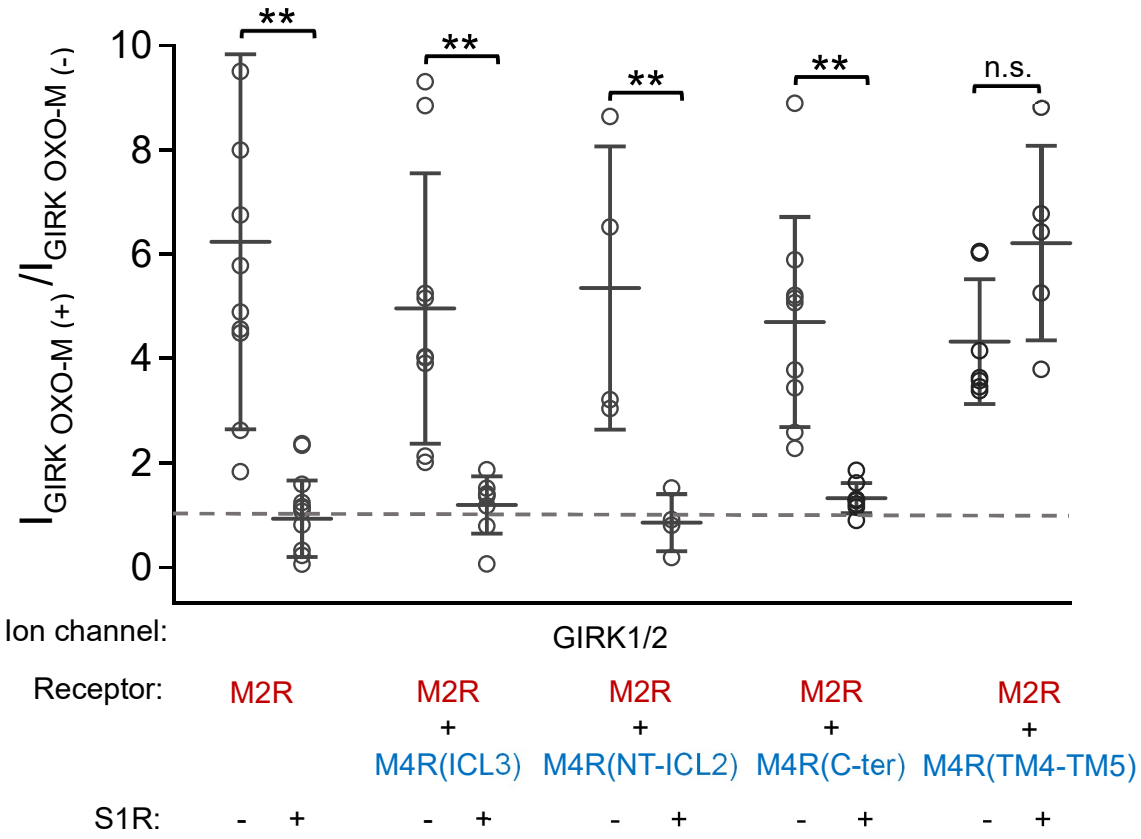

Fig. 14 The regulation of various chimeras between M2R and M4R by S1R measured by GIRK1/2 current

Comparison of the ratio of the GIRK1/2 current before and after application of their own agonists in GIRK1/2+M2R, GIRK1/2+M2R/M4R(ICL3), GIRK1/2+M2R/M4R(NT-ICL2), GIRK1/2+M2R/M4R(C-ter) and GIRK1/2+M2R/M4R(TM4-TM5) without or with S1R co-transfected cells. Data are mean ± SD (n=4-12). Student's *t*-test (Unpaired), ** indicates $P<0.01$.

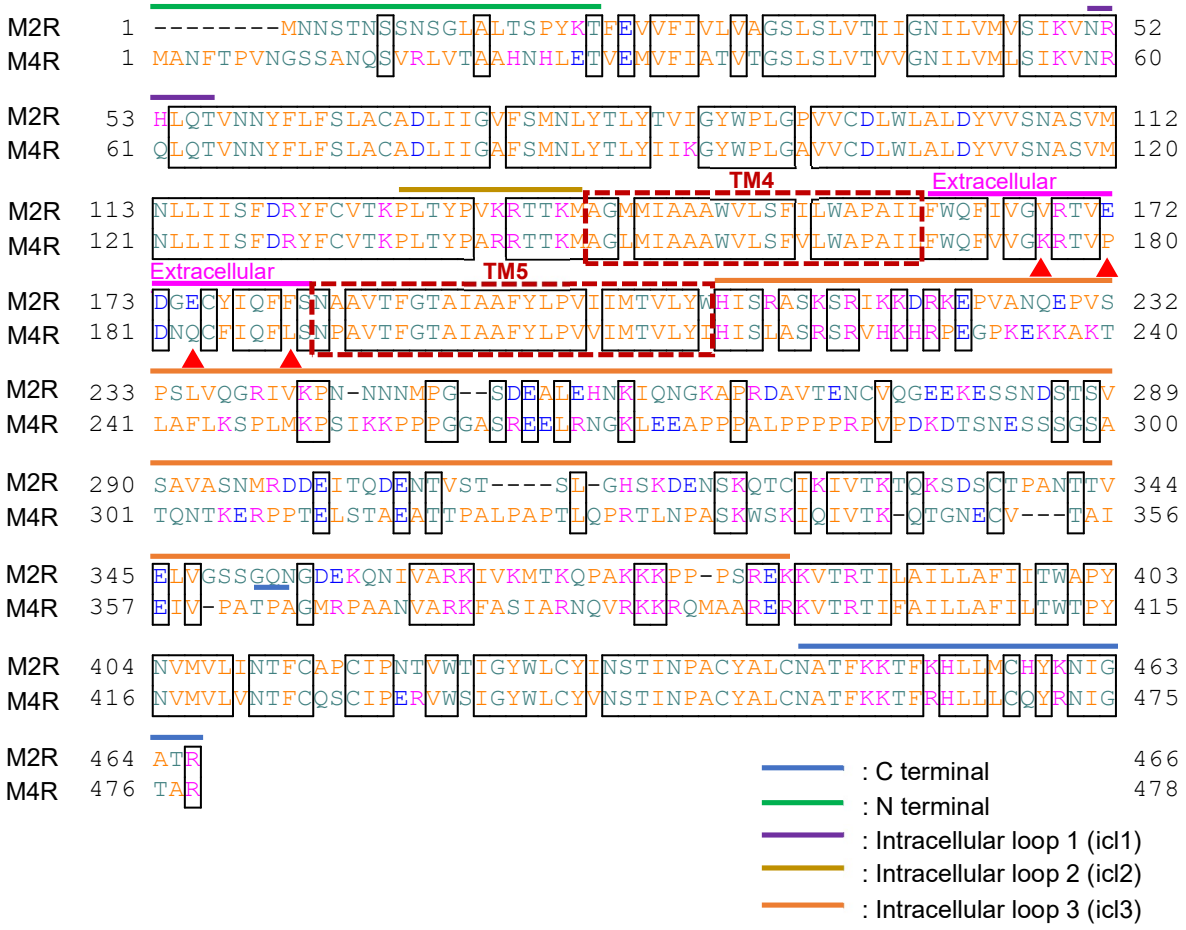

Fig. 15 The alignment of amino acid sequence of M2R and M4R

The full amino acid sequence of porcine M2R and rat M4R are aligned. Red dotted lines indicate TM4 and TM5 of M2R and M4R. Arrows indicate the position of examined single point mutations in the extracellular loop between TM4 and TM5.

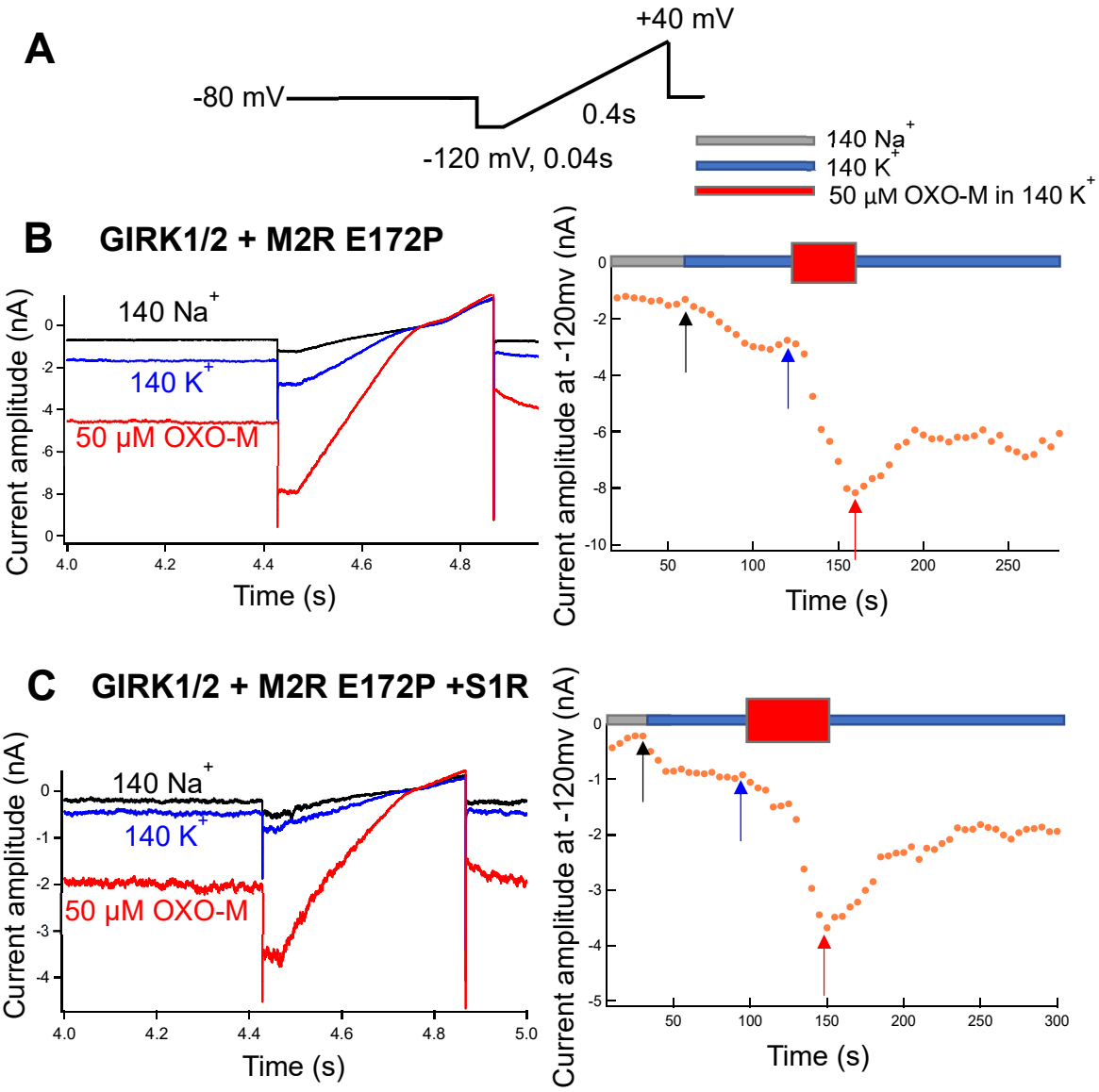

Fig. 16 The regulation of M2R E172P by S1R measure by GIRK1/2 current

(A) A voltage ramp pulse protocol used in the whole cell patch-clamp recording. (B) Recordings from GIRK1/2 and M2R E172P transfected HEK293T cells. (C) Recordings from GIRK1/2, M2R E172P and S1R transfected HEK293T cells. Left panels in (B) and (C): Representative current traces evoked by ramp pluses in $140Na^+$ (Black), $140K^+$ (Blue) and $140K^+$ with 50µM OXO-M (Red), respectively. Right panels in (B) and (C): Timelapse change of the current amplitude at -120mV in different bath solutions. Black, blue and red arrows indicate the time points of representative current traces shown in the left panel in $140Na^+$, $140K^+$ and $140K^+$ with 50µM OXO-M, respectively.

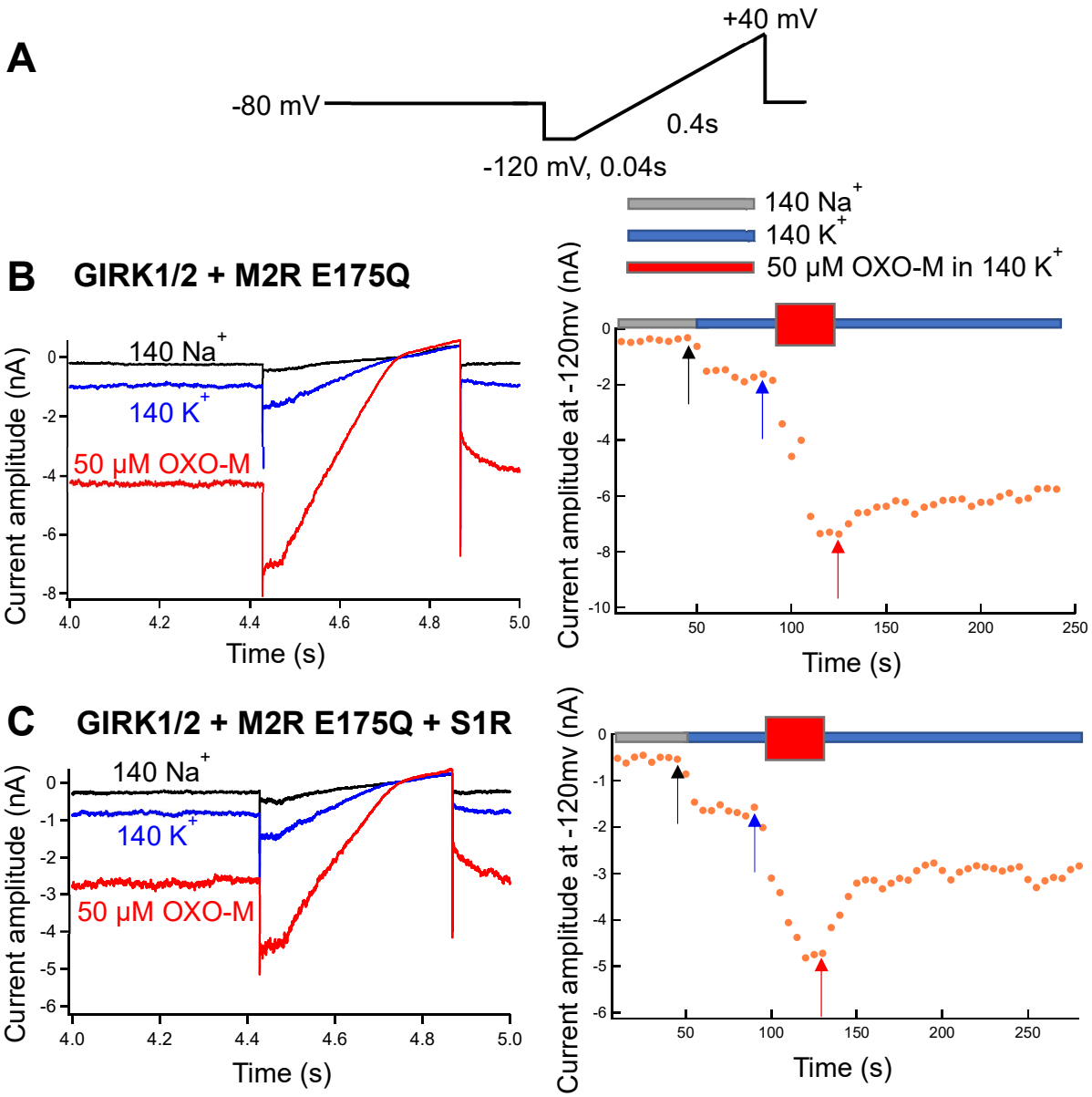

Fig. 17 The regulation of M2R E175Q by S1R measure by GIRK1/2 current

(A) A voltage ramp pulse protocol used in the whole cell patch-clamp recording. (B) Recordings from GIRK1/2 and M2R E175Q transfected HEK293T cells. (C) Recordings from GIRK1/2, M2R E175Q and S1R transfected HEK293T cells. Left panels in (B) and (C): Representative current traces evoked by ramp pluses in $140Na^+$ (Black), $140K^+$ (Blue) and $140K^+$ with 50μM OXO-M (Red), respectively. Right panels in (B) and (C): Timelapse change of the current amplitude at -120mV in different bath solutions. Black, blue and red arrows indicate the time points of representative current traces shown in the left panel in $140Na^+$, $140K^+$ and $140K^+$ with 50μM OXO-M, respectively.

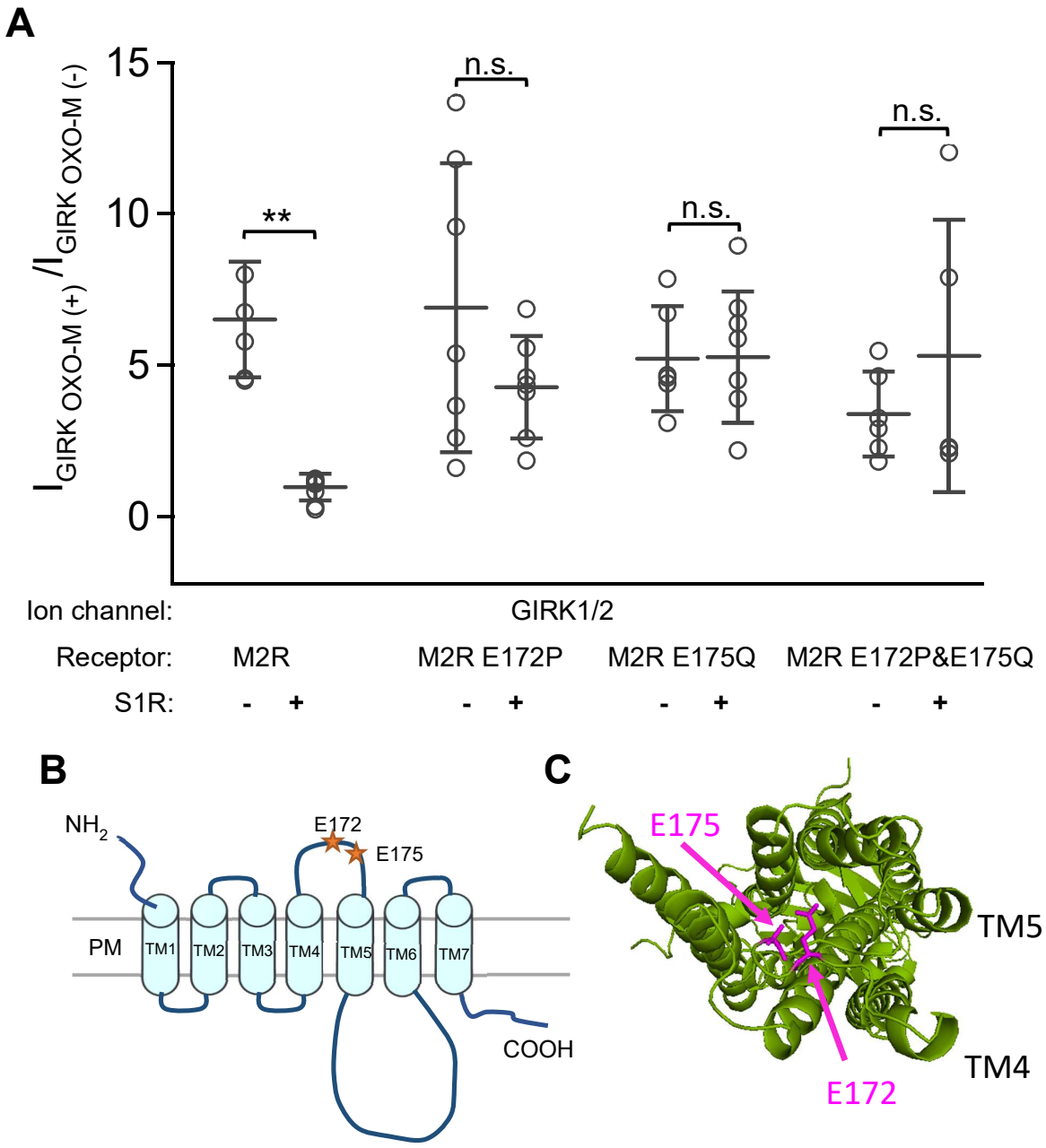

Fig. 18 Regulation on GIRK1/2 current by S1R through M2R and its mutants

(A) Comparison of the ratio of the GIRK1/2 current before and after application of OXO-M in GIRK1/2+M2R, GIRK1/2+M2R E172P±S1R, GIRK1/2+M2R E175Q±S1R, GIRK1/2+M2R+ E172P/E175Q±S1R transfected cells. Data are mean ± SD (n=4-7). Student's *t*-test (Unpaired), ** indicates $P<0.01$. (B) A schematic view of M2R, orange asterisks indicate the location of E172, E175 on M2R. (C) Top view from the extracellular side of the crystal structure of M2R (Human M2R, 4MQS). Magenta color depicts the location of E172 and E175 using PyMOL.

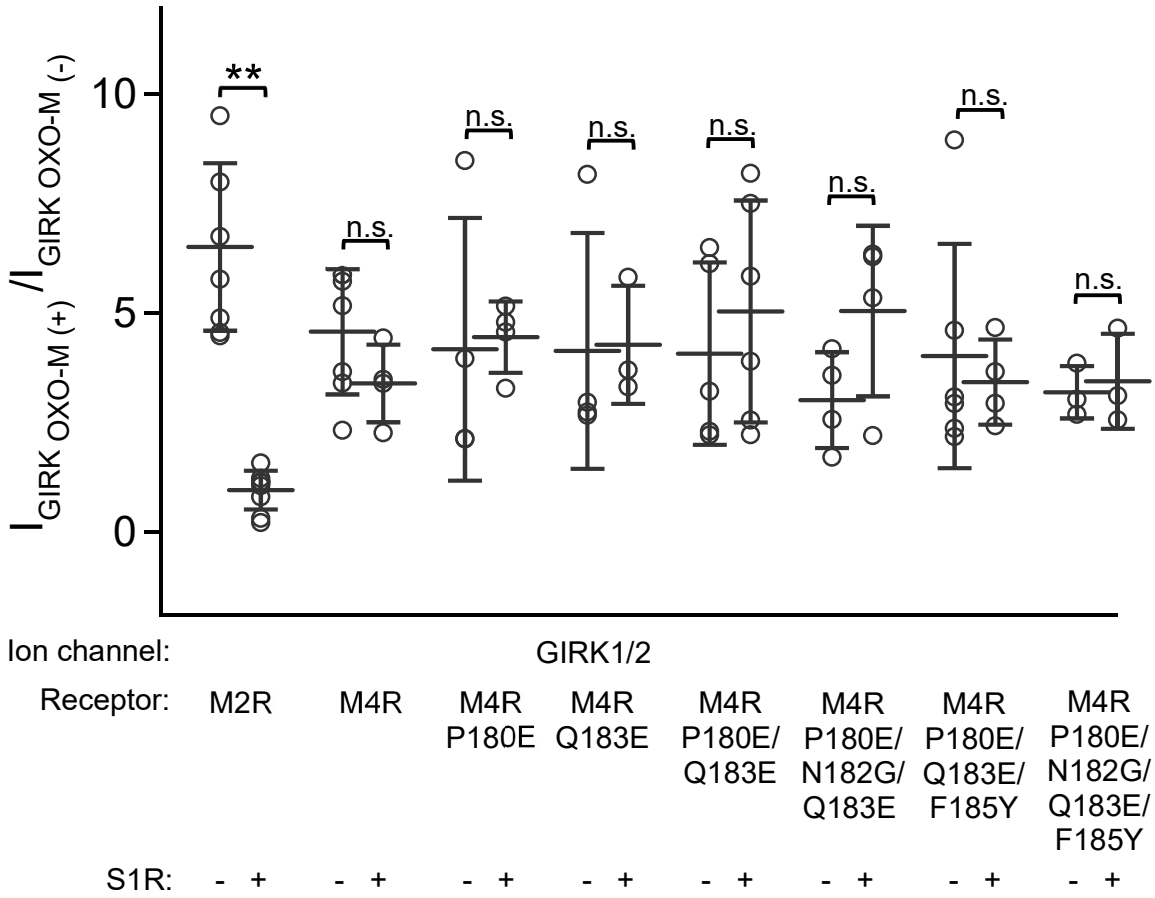

Fig. 19 The regulation of GIRK1/2 and M4R mutants by S1R

Comparison of the ratio of the GIRK1/2 current before and after application of OXO-M in GIRK1/2+M2R±S1R, GIRK1/2+M4R±S1R, GIRK1/2+M4R P180E±S1R, GIRK1/2+M4R Q183E±S1R, GIRK1/2+M4R P180E/Q183E±S1R, GIRK1/2+M4R P180E/N182G/Q183E±S1R, GIRK1/2+M4R P180E/Q183E/F185Y±S1R and GIRK1/2+M4R P180E/N182G/Q183E/F185Y±S1R transfected HEK293T cells. Data are mean ± SD (n=4-7). Student's *t*-test (Unpaired), ** indicates $P<0.01$.

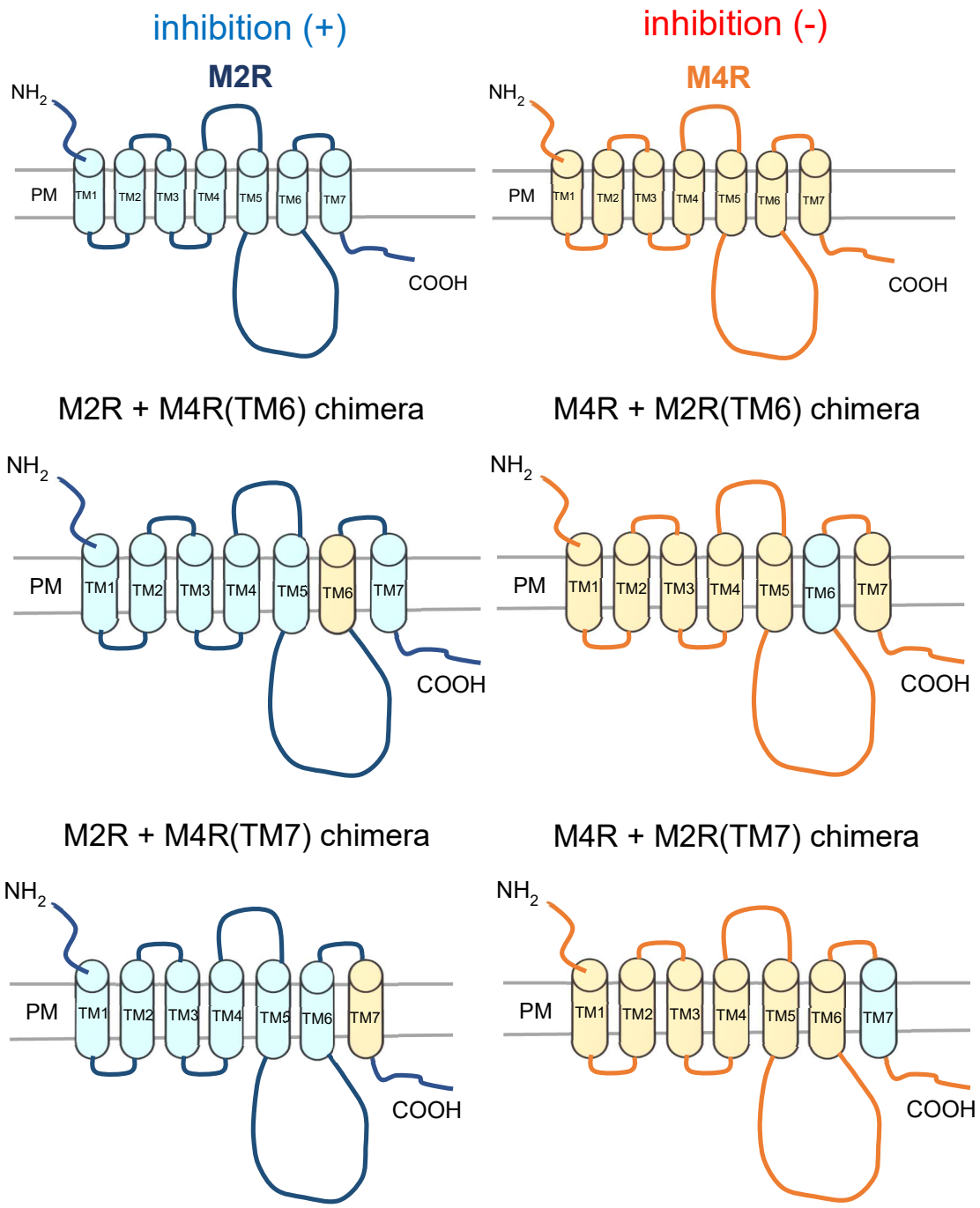

Fig. 20 Schematic drawings of chimeras between M2R and M4R

(Top panel) Topological models of M2R WT is indicated in blue and that of M4R WT is indicated in yellow. (Middle panel) TM6 segment was swapped between M2R and M4R. (Bottom panel) TM7 part was swapped between M2R and M4R.

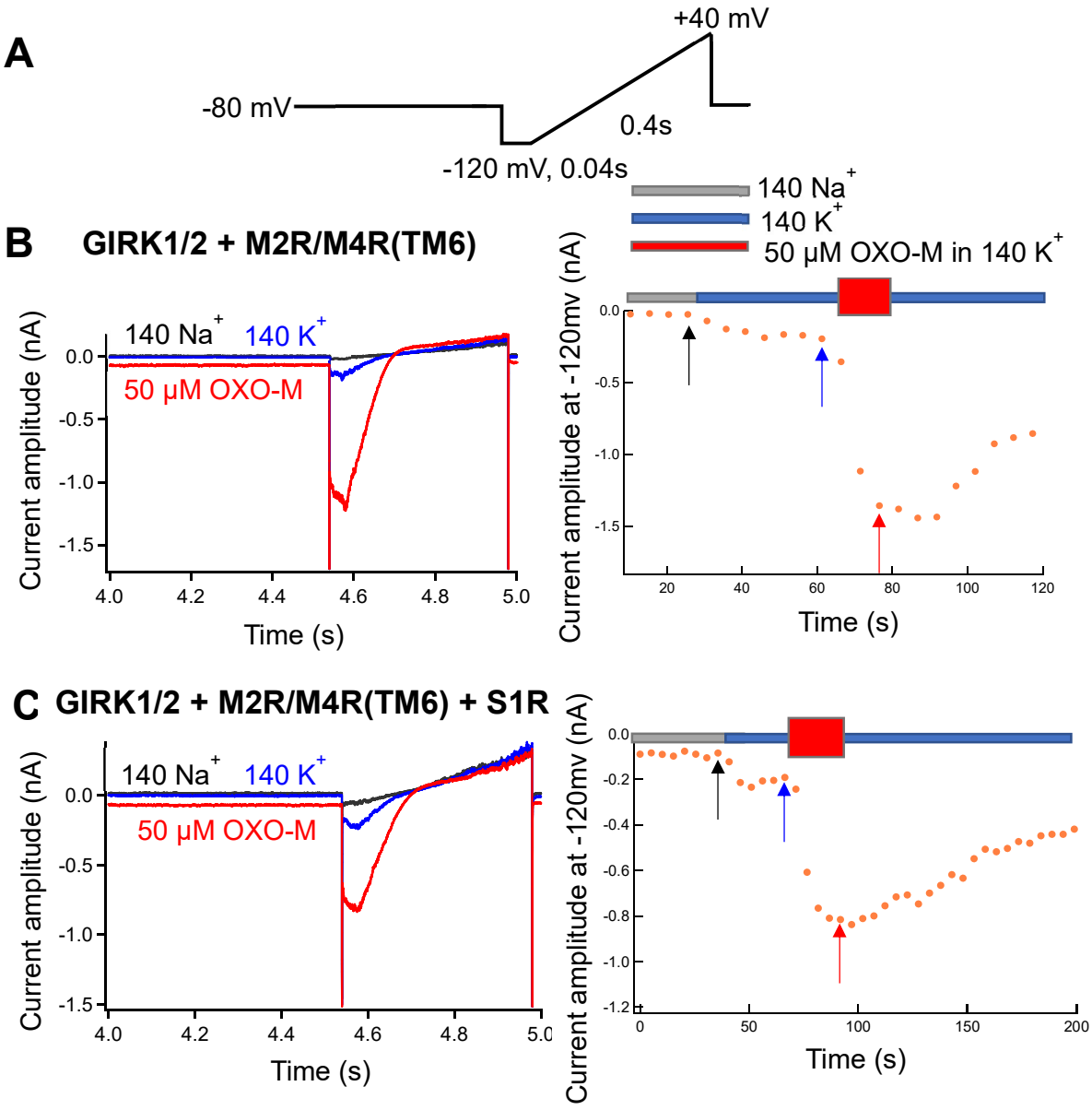

Fig. 21 The regulation M2R/M4R(TM6) chimera by S1R measured by GIRK1/2 current

(A) A voltage ramp pulse protocol used in the whole cell patch-clamp recording. (B) Recordings from GIRK1/2 and M2R/M4R(TM6) transfected HEK293T cells. (C) Recordings from GIRK1/2, M2R/M4R(TM6) and S1R transfected HEK293T cells. Left panels in (B) and (C): Representative current traces evoked by ramp pulses in $140Na^+$ (Black), $140K^+$ (Blue) and $140K^+$ with 50μM OXO-M (Red), respectively. Right panels in (B) and (C): Timelapse change of the current amplitude at -120mV in different bath solutions. Black, blue and red arrows indicate the time points of representative current traces shown in the left panel in $140Na^+$, $140K^+$ and $140K^+$ with 50μM OXO-M, respectively.

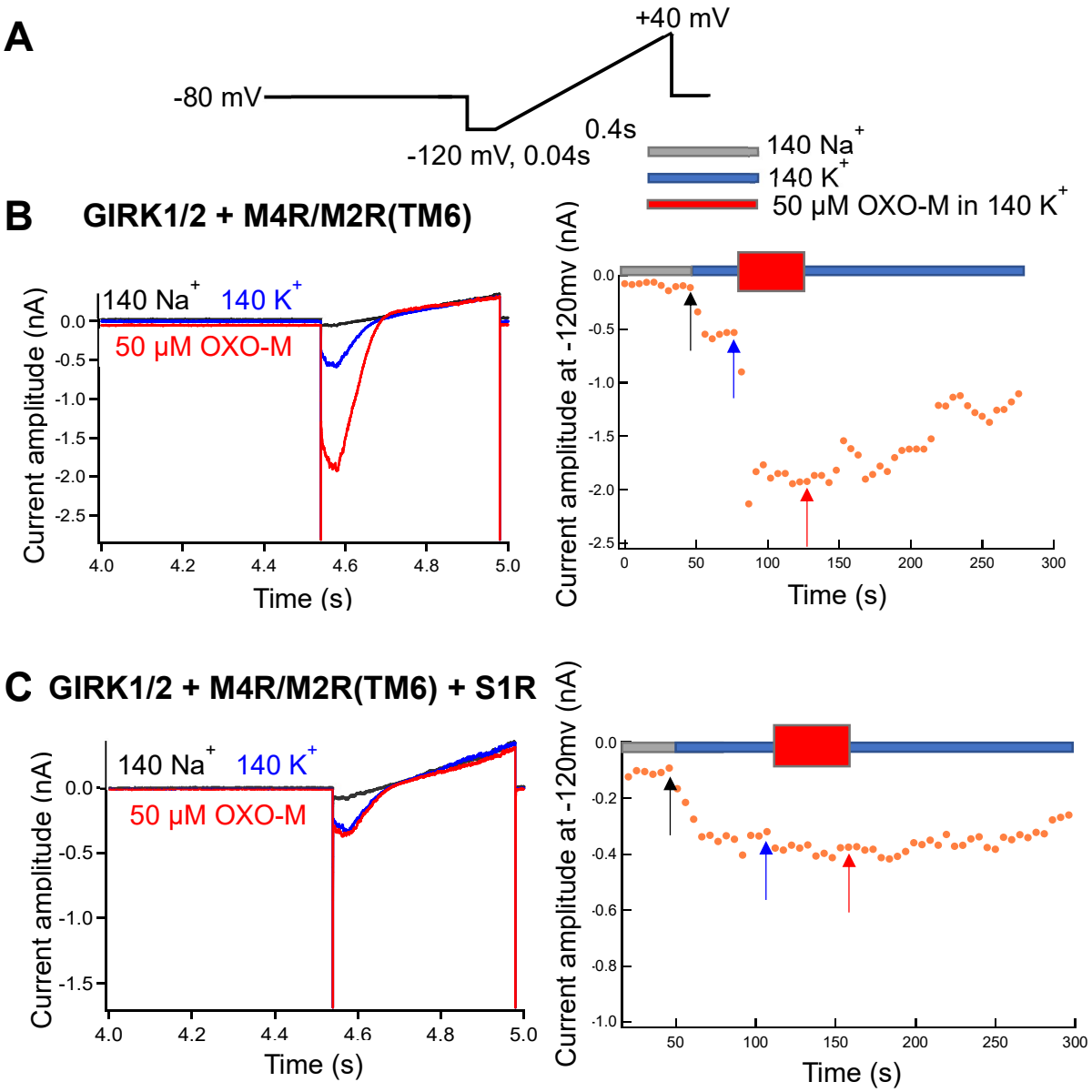

Fig. 22 The regulation of M4R/M2R(TM6) chimera by S1R measured by GIRK1/2 current

(A) A voltage ramp pulse protocol used in the whole cell patch-clamp recording. (B) Recordings from GIRK1/2 and M4R/M2R(TM6) transfected HEK293T cells. (C) Recordings from GIRK1/2, M4R/M2R(TM6) and S1R transfected HEK293T cells. Left panels in (B) and (C): Representative current traces evoked by ramp pulses in $140Na^+$ (Black), $140K^+$ (Blue) and $140K^+$ with 50μM OXO-M (Red), respectively. Right panels in (B) and (C): Timelapse change of the current amplitude at -120mV in different bath solutions. Black, blue and red arrows indicate the time points of representative current traces shown in the left panel in $140Na^+$, $140K^+$ and $140K^+$ with 50μM OXO-M, respectively.

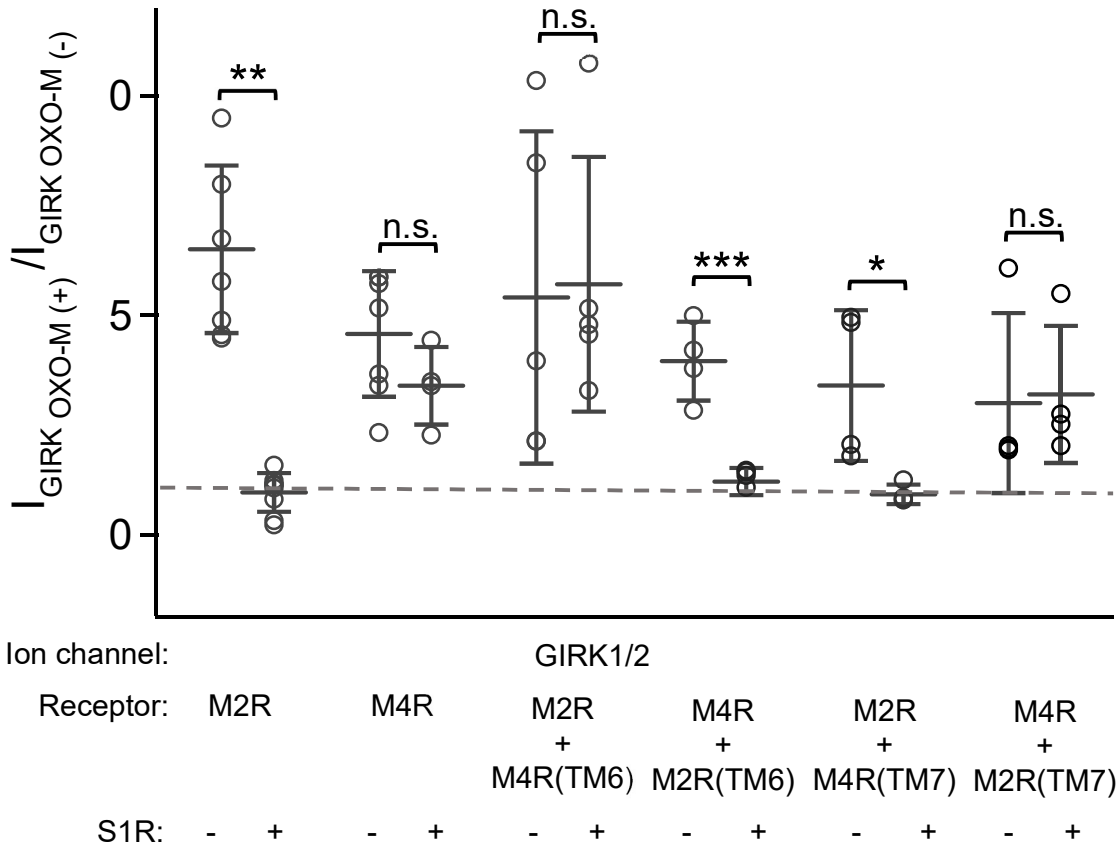

Fig. 23 The regulation of GIRK1/2 and M2R/M4R chimeras by S1R

Comparison of the ratio of the GIRK1/2 current before and after application of OXO-M in GIRK1/2+M2R±S1R, GIRK1/2+M4R±S1R, GIRK1/2+M2R/M4R(TM6)±S1R, GIRK1/2+M4R/M2R(TM6)±S1R, GIRK1/2+M2R/M4R(TM7)±S1R and GIRK1/2+M4R/M2R(TM7)±S1R transfected HEK293T cells. Data are mean ± SD (n=4-7). Student's *t*-test (Unpaired), * indicates $P<0.05$, ** indicates $P<0.01$, *** indicates $P<0.001$.

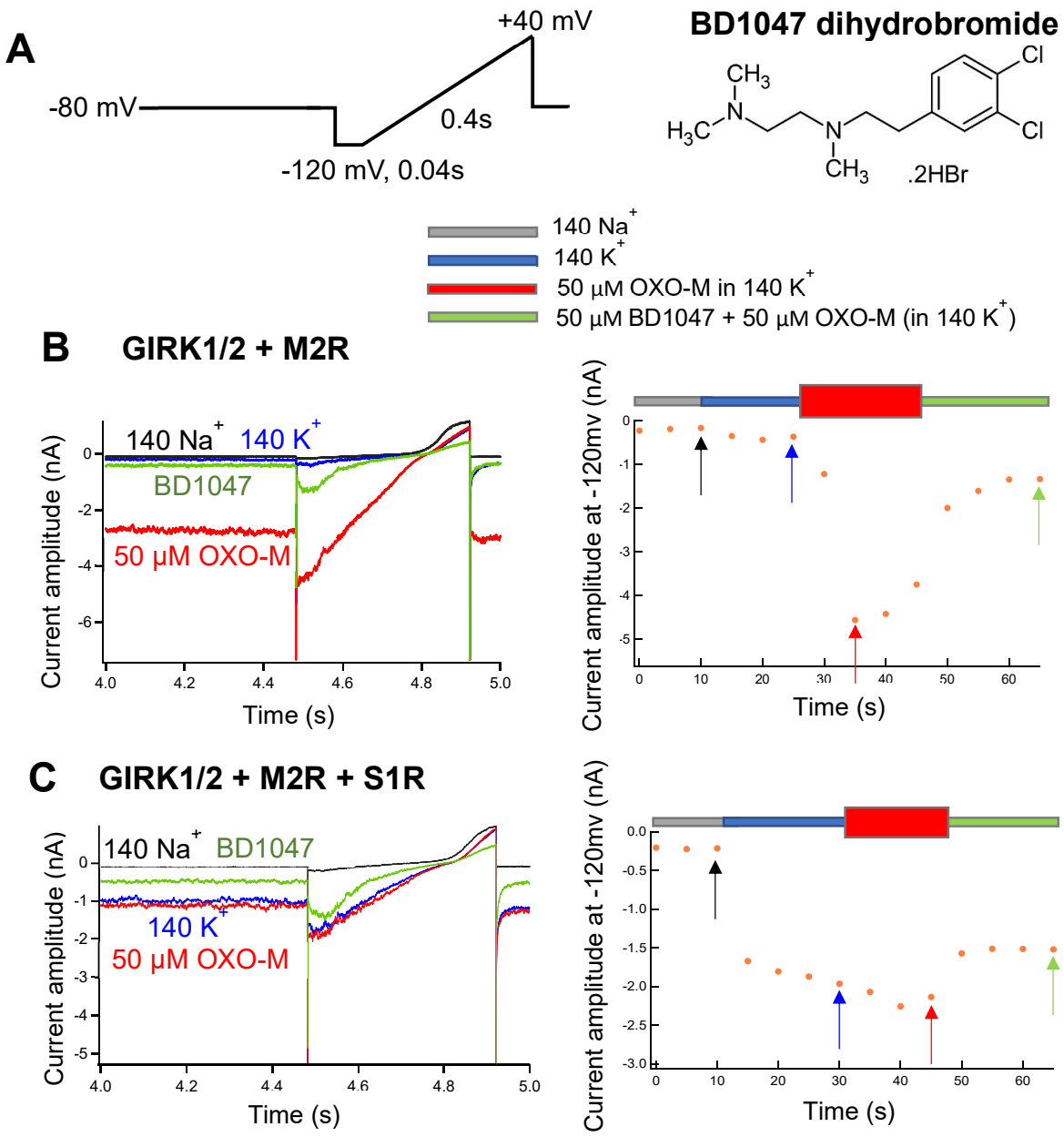

Fig. 24 The regulation of GIRK1/2 and M2R by S1R

(A) Left panel: A voltage ramp pulse protocol used in the whole cell patch-clamp recording. Right panel: The chemical structure of BD1047, an antagonist of S1R. (B) Recordings from GIRK1/2 and M2R transfected HEK293T cells. (C) Recordings from GIRK1/2, M2R and S1R transfected HEK293T cells. Left panels in (B) and (C): Representative current traces evoked by ramp pulses in $140Na^+$ (Black), $140K^+$ (Blue), $140K^+$ with 50μM OXO-M (Red), $140K^+$ with both 50μM OXO-M and 50μM BD (Green), respectively. Right panels in (B) and (C): Timelapse changes of the current amplitude at -120mV in different bath solutions. Black, blue, red and green arrows indicate the time points of representative current traces shown in the left panel in $140Na^+$, $140K^+$, $140K^+$ with 50μM OXO-M and $140K^+$ with both 50μM OXO-M and 50μM BD, respectively.

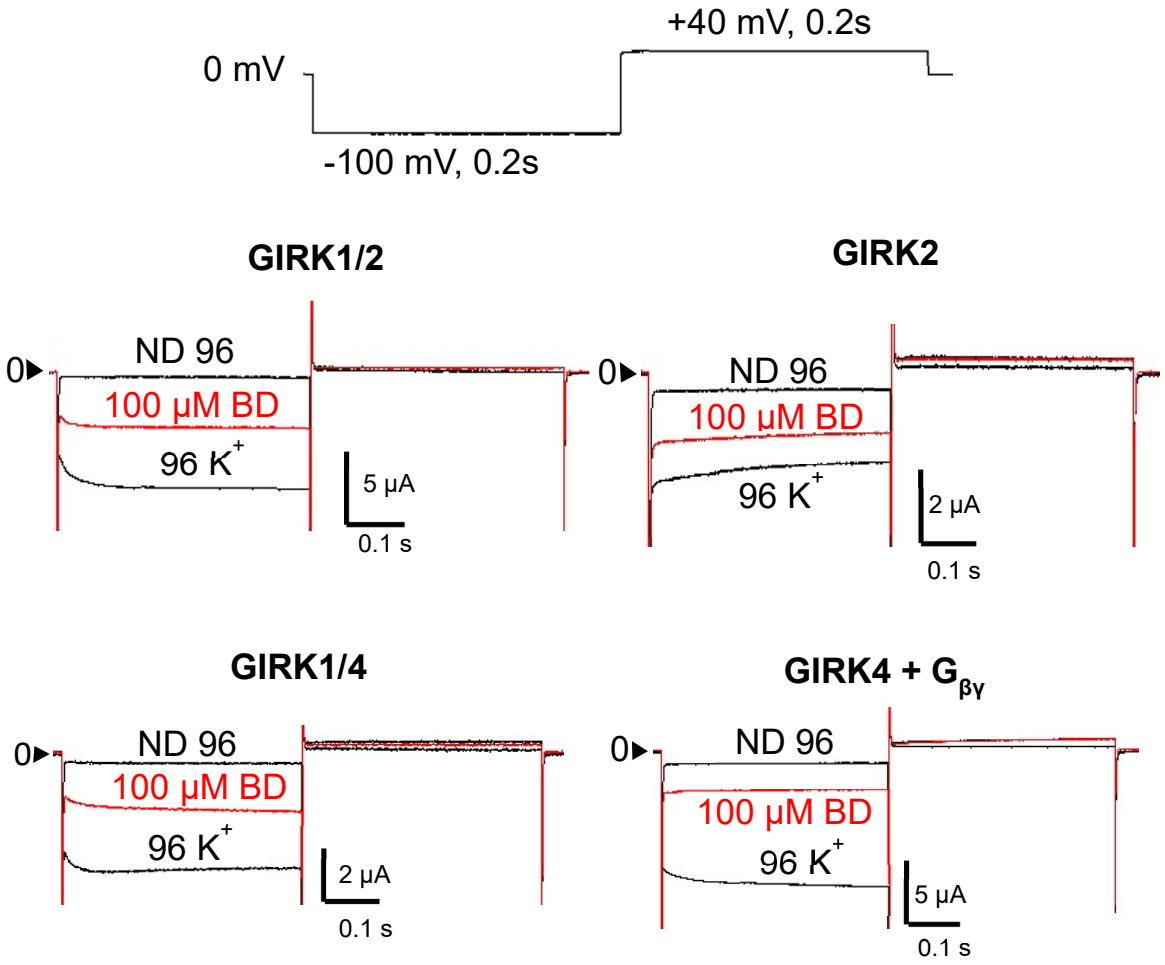

Fig. 25 The effects of BD1047 on GIRK channels

Representative current recordings from Xenopus oocytes expressed only with GIRK1/2, GIRK2, GIRK1/4 or GIRK4 in ND96, $96K^+$ and $96K^+$ with 100 μM BD1047 respectively evoked by the voltage protocol shown above.

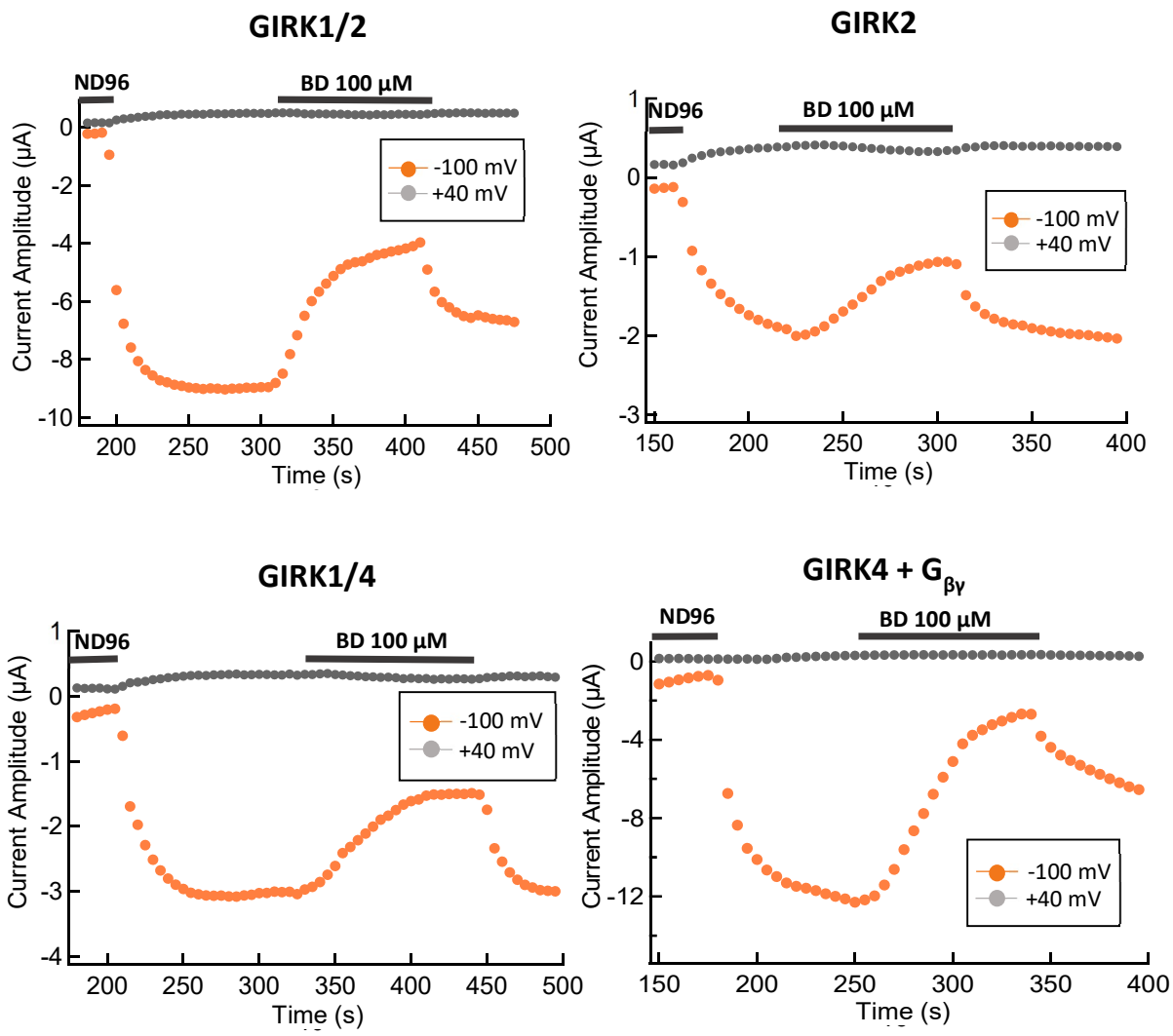

Fig. 26 The effects of BD1047 on GIRK channels presented as timelapse changes

The timelapse changes of the current amplitudes at -100 mV (orange plots) in the absence and then the presence of BD1047 (100 µM) in 96K^+ solution in oocytes expressing GIRK1/2, GIRK2, GIRK1/4 and GIRK4 channels. BD1047 was applied and washed out by constant bath perfusion using a peristatic pump.

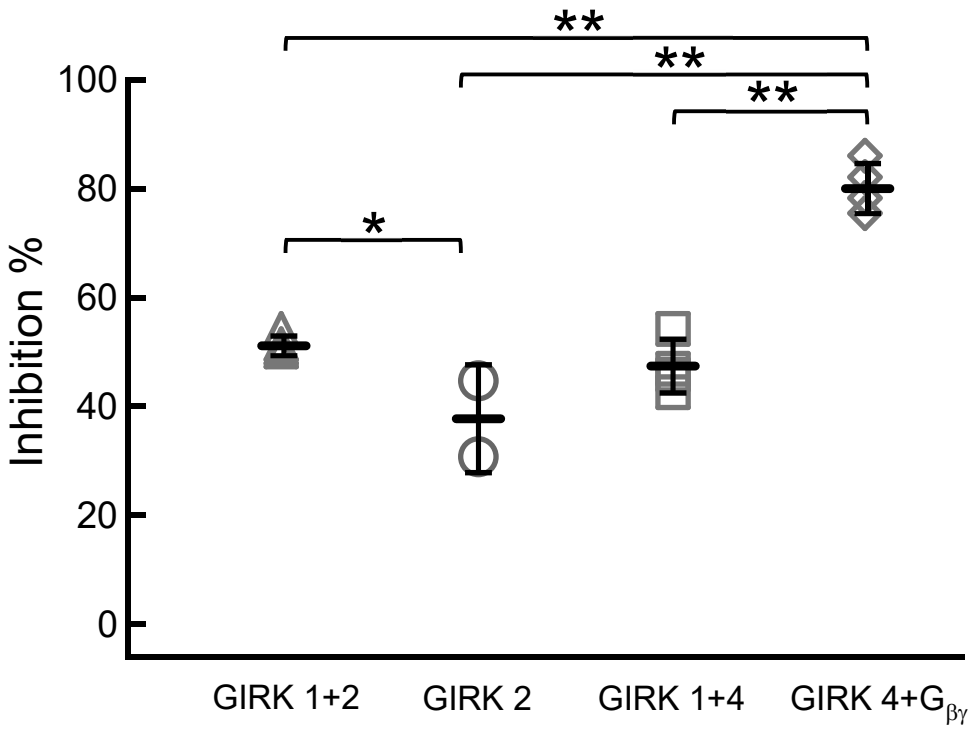

Fig. 27 The effects of BD1047 on GIRK channels

Comparison of the inhibition percentages, before and after the application of 100μM BD1047, of GIRK1/2, GIRK2, GIRK1/4 and GIRK4 current. Data are mean ± SD (n = 5 for each); One way ANOVA followed by Tukey's test, * indicates $P<0.05$; ** indicates $P<0.01$.

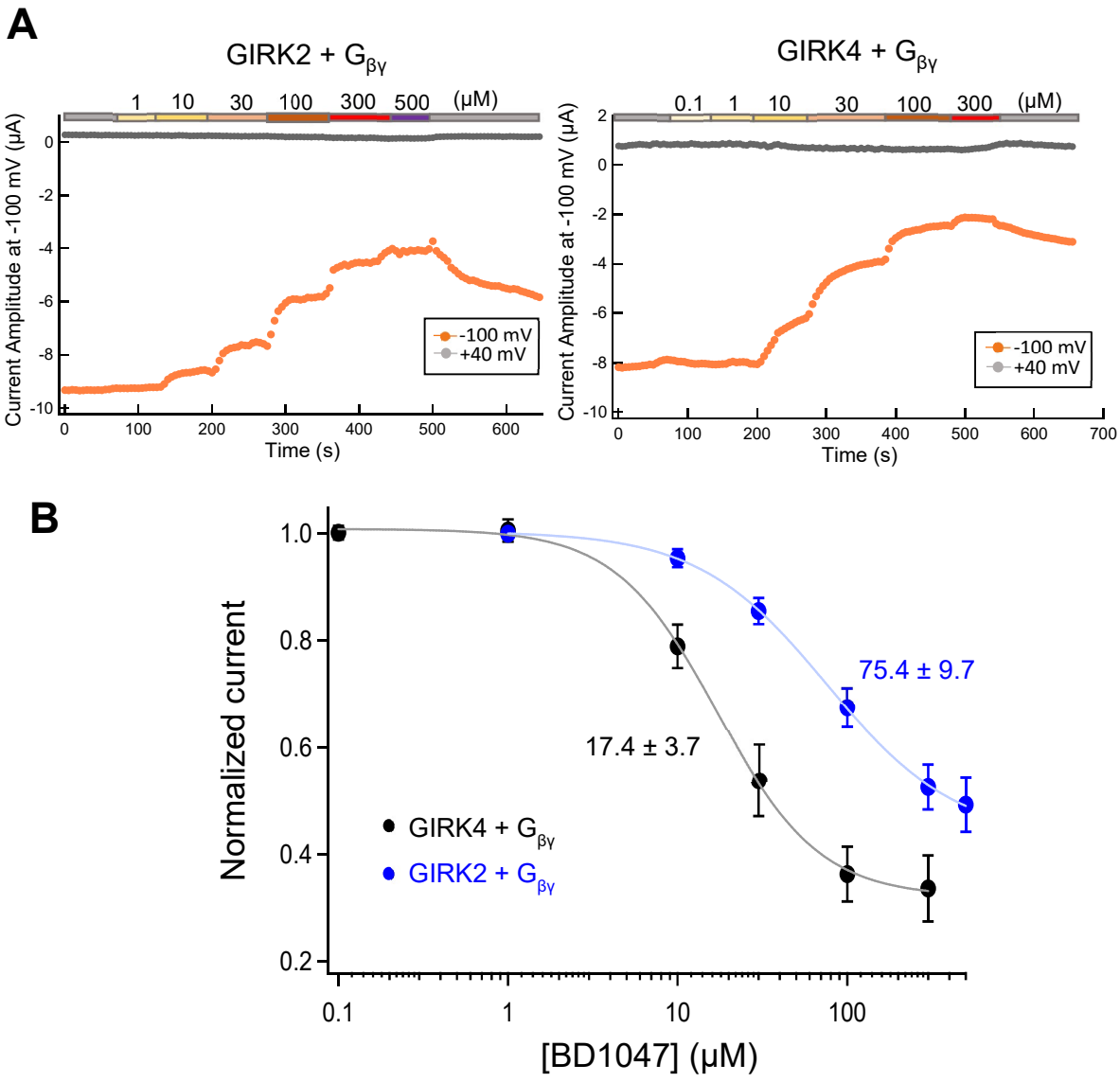

Fig. 28 Dose inhibition relationships of BD 1047 on GIRK2 and GIRK4 current

(A) The time courses of the current changes in various concentrations of BD1047 in oocytes expressing GIRK2 or GIRK4 channel. Orange dots indicate the recorded current amplitudes at -100mV and gray dots indicate those at +40mV. (B) Dose response relationships of BD1047 on GIRK2 (blue) and GIRK4 channel (black). Data are mean ± SD (n = 4-5) for each plot. IC_{50} is 75.4 ± 9.7 (μM) (GIRK2) and 17.4 ± 3.7(μM) (GIRK4), respectively.

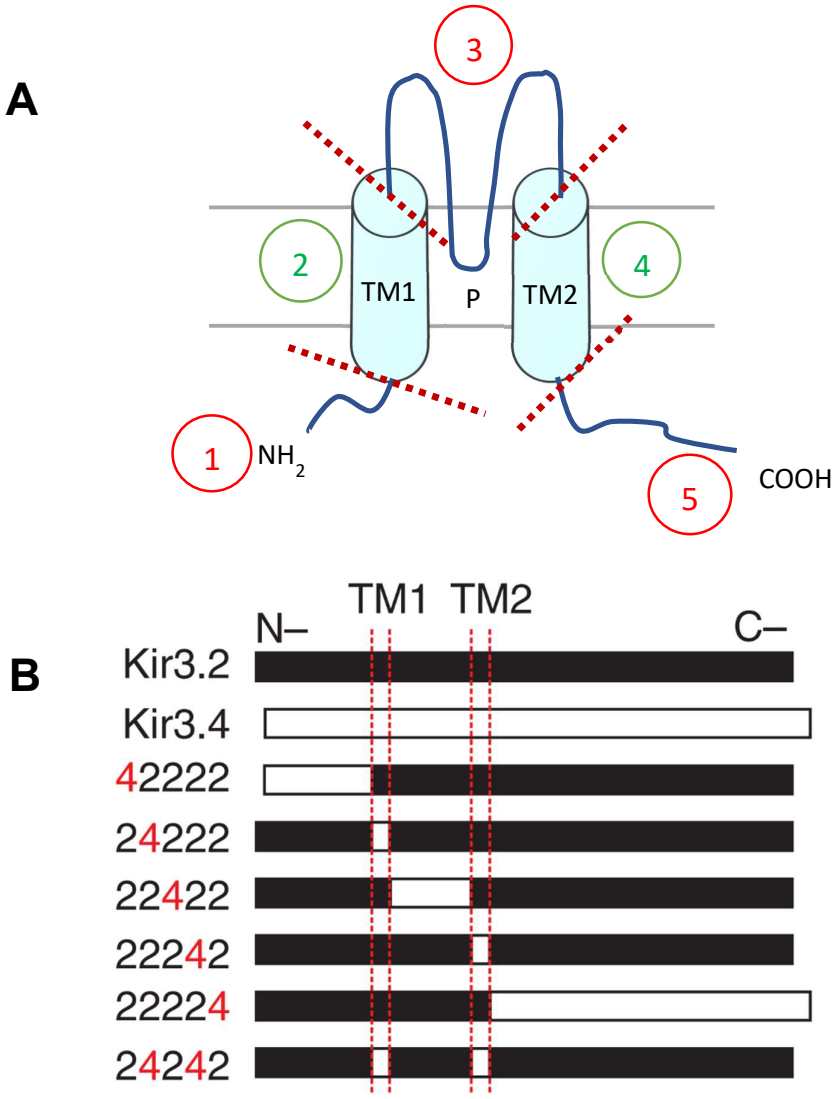

(cited from Fig. 7B of Chen et al., 2017)

Fig. 29 Schematic drawings of chimeras between GIRK2 and GIRK4

(A) GIRK2 was divided into five parts (N-ter, TM1, the pore forming loop between TM1 and TM2, TM2 and C-ter) and each of all parts was replaced with the corresponding part from GIRK4. (B) Schematic drawing of six chimeras, GIRK42222, GIRK24222, GIRK22422, GIRK22242, GIRK22224 and GIRK24242, provided by Dr. Chen (Chen et al, 2017). Red letters "4" indicate those swapped to the corresponding part from GIRK4.

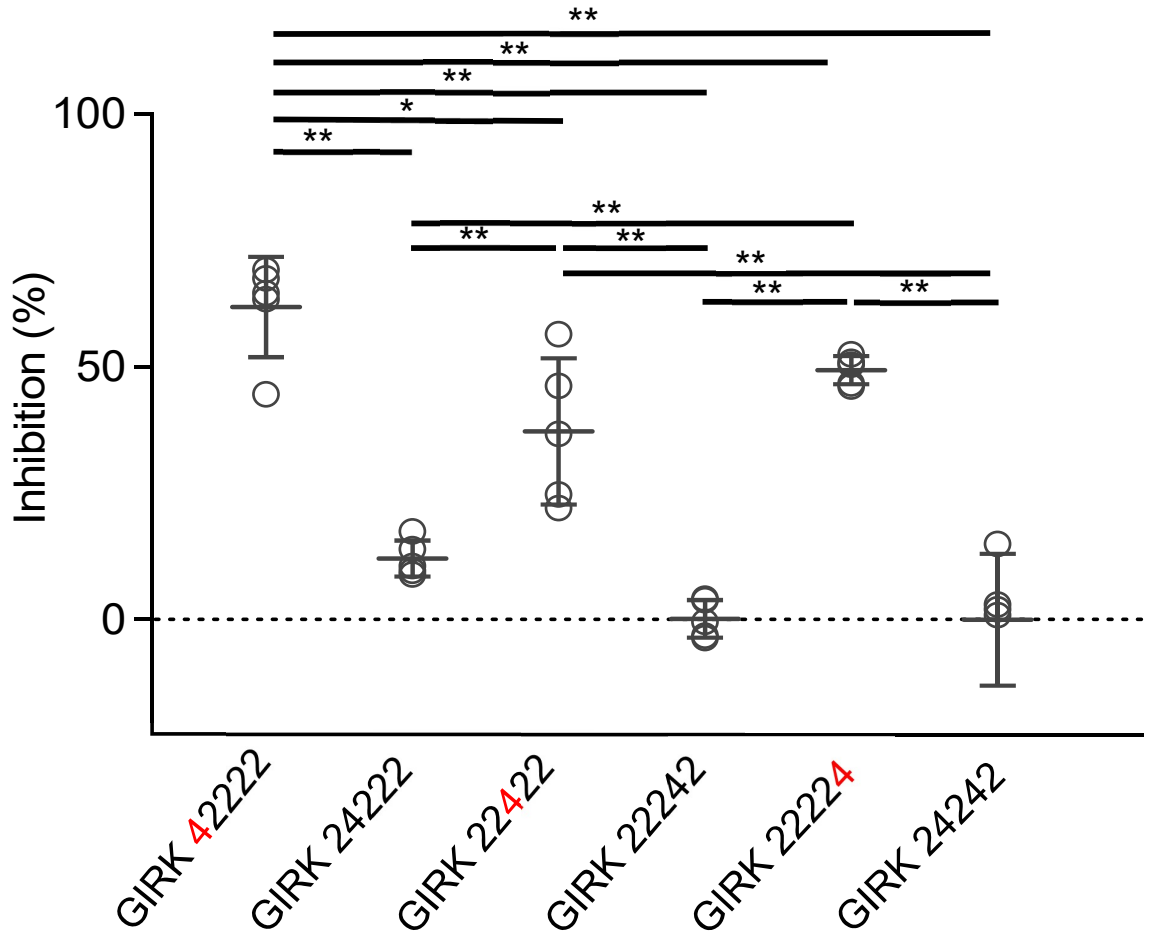

Fig. 30 The effects of BD1047 (100μM) on GIRK2/4 chimeras

Comparison of the inhibition percentages before and after the application of 100 μM BD1047 on GIRK42222, GIRK24222, GIRK22422, GIRK22242, GIRK22224 and GIRK24242 chimeras. Data are mean ± SD (n = 5 for each); One way ANOVA followed by Tukey's test, * indicates $P<0.05$; ** indicates $P<0.01$.

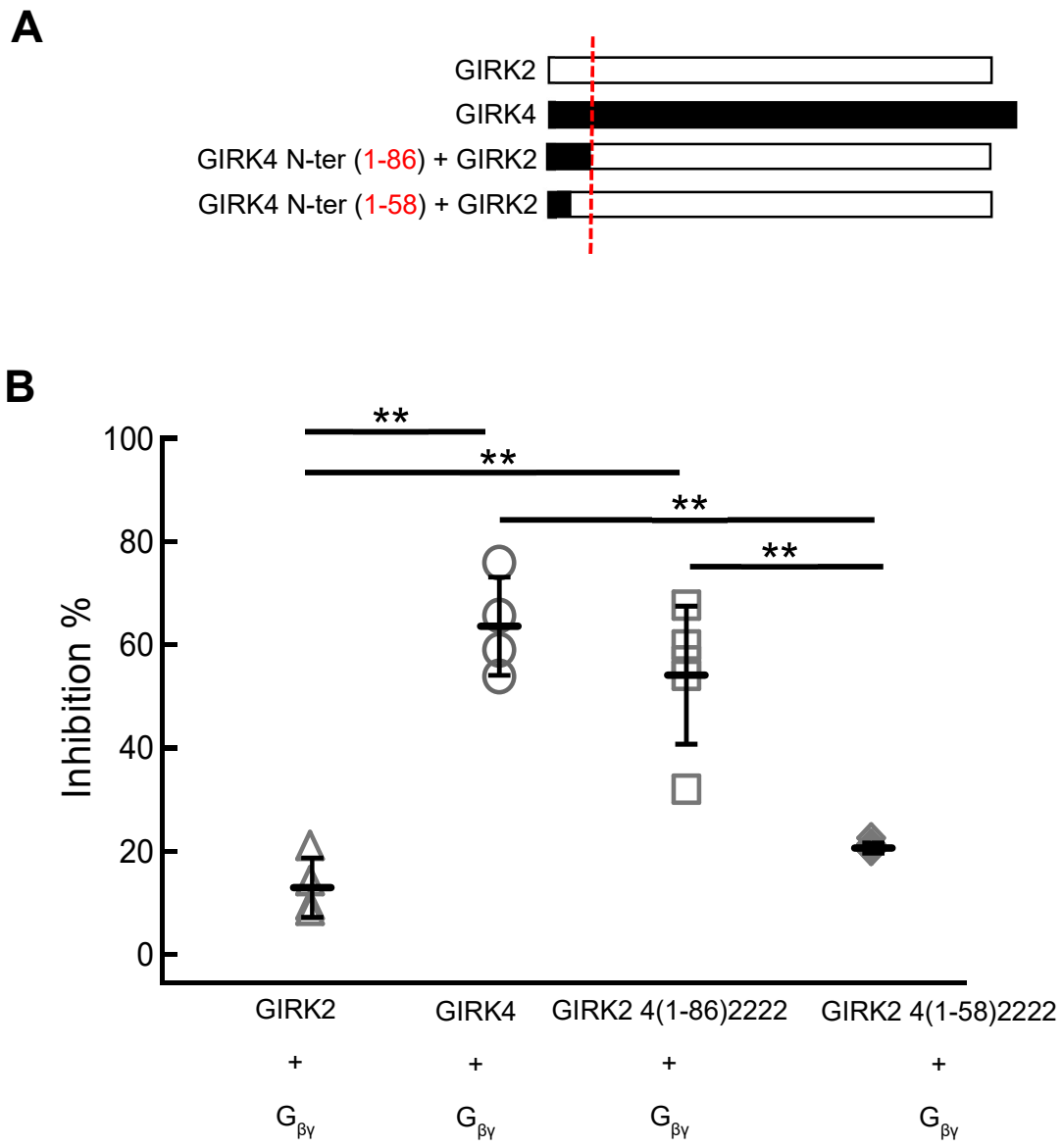

Fig. 31 The effects of BD1047 on GIRK2/4 N-ter chimeras

(A) Schematic drawings of GIRK2/4 N-ter chimeras. GIRK2 4(1-86)2222 includes the whole 86 amino acids of N-ter from GIRK4, and GIRK2 4(1-58)2222 includes the distal 58 amino acids of N-ter from GIRK4. (B) Comparison of the inhibition percentages before and after the application of 100μM BD1047 on GIRK2, GIRK4, GIRK2 4(1-86)2222 and GIRK2 4(1-58)2222. Data are mean ± SD (n = 4-5 for each); One way ANOVA followed by Tukey's test, ** indicates $P<0.01$.

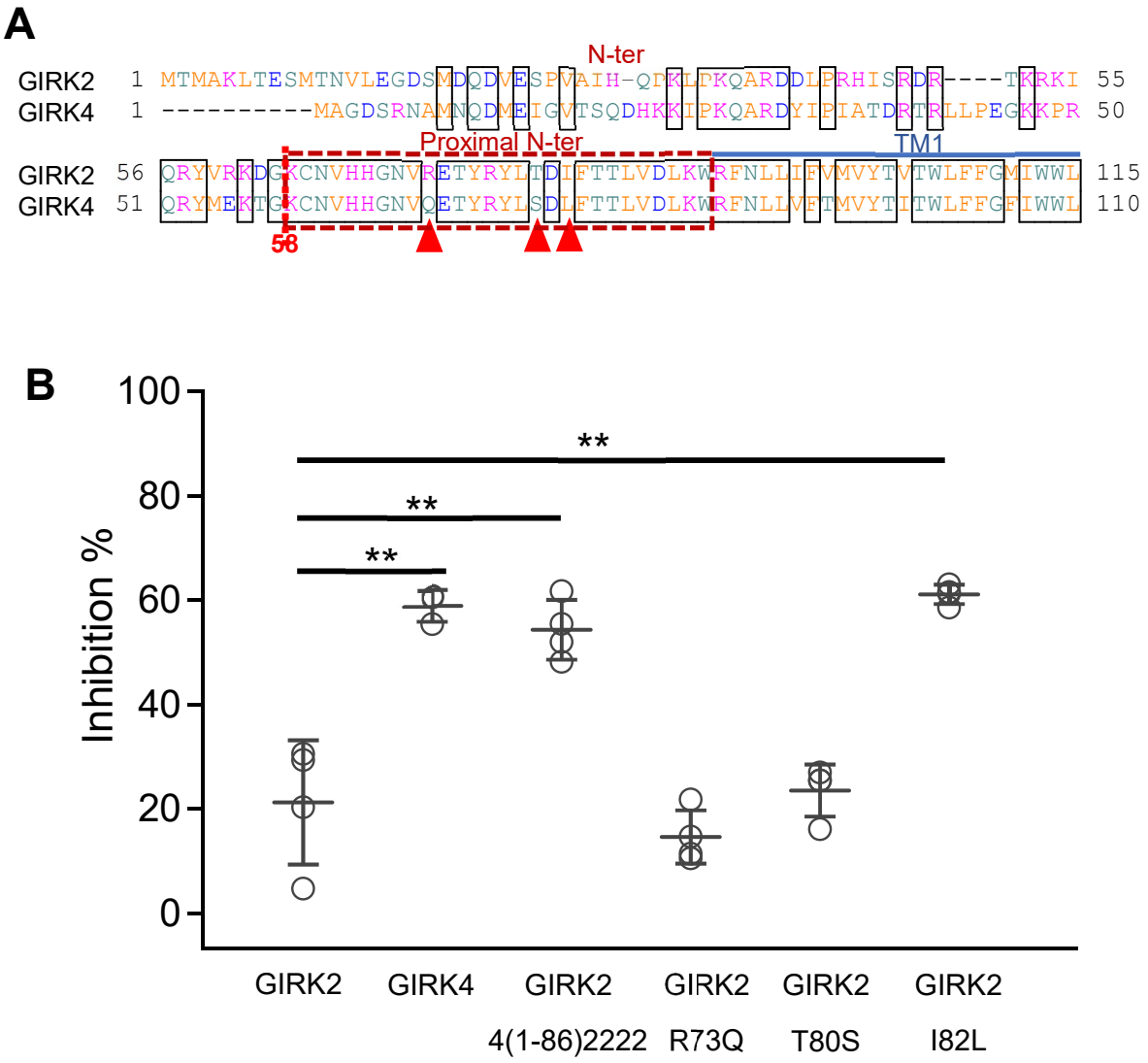

Fig. 32 The effects of BD 1047 on GIRK2/4 chimeras and mutants

(A) The amino acid sequence alignment of N-ter of mouse GIRK2 and rat GIRK4. A red dotted frame indicates the proximal N-ter of GIRK2 and GIRK4. Red arrows indicated non-conserved amino acids in the proximal N-ter region. (B) Comparison of the inhibition percentages before and after the application of 100μM BD1047 on GIRK2, GIRK4, GIRK2 4(1-86)2222, GIRK2 R73Q, GIRK2 T80S and GIRK2 I82L. Data are mean ± SD (n = 4-5 for each); One way ANOVA followed by Tukey's test, $^{**}P<0.01$.

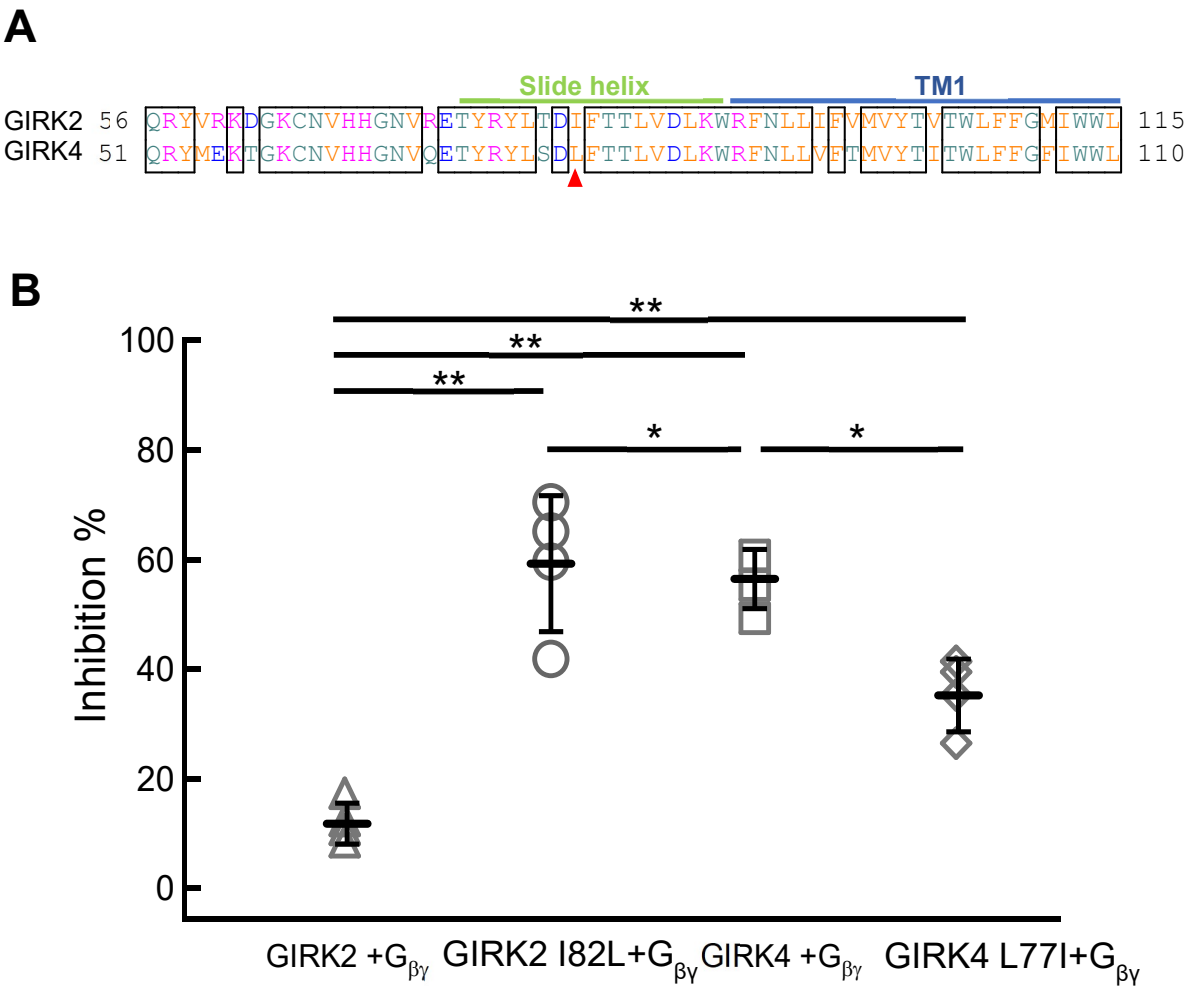

Fig. 33 The effects of BD1047 on GIRK2 and GIRK4 mutants

(A) The amino acid sequence alignment of N-terminal of mouse GIRK2 and rat GIRK4. A red arrow indicates Leu77 of GIRK4, an amino acid residue corresponding to Ile82 of GIRK2. (B) Comparison of the inhibition percentages before and after the application of 100μM BD1047 on GIRK2, GIRK2 I82L, GIRK4 and GIRK L77I. Data are mean ± SD (n = 4 for each); One way ANOVA followed by Tukey's test, * indicates $P<0.05$; ** indicates $P<0.01$.

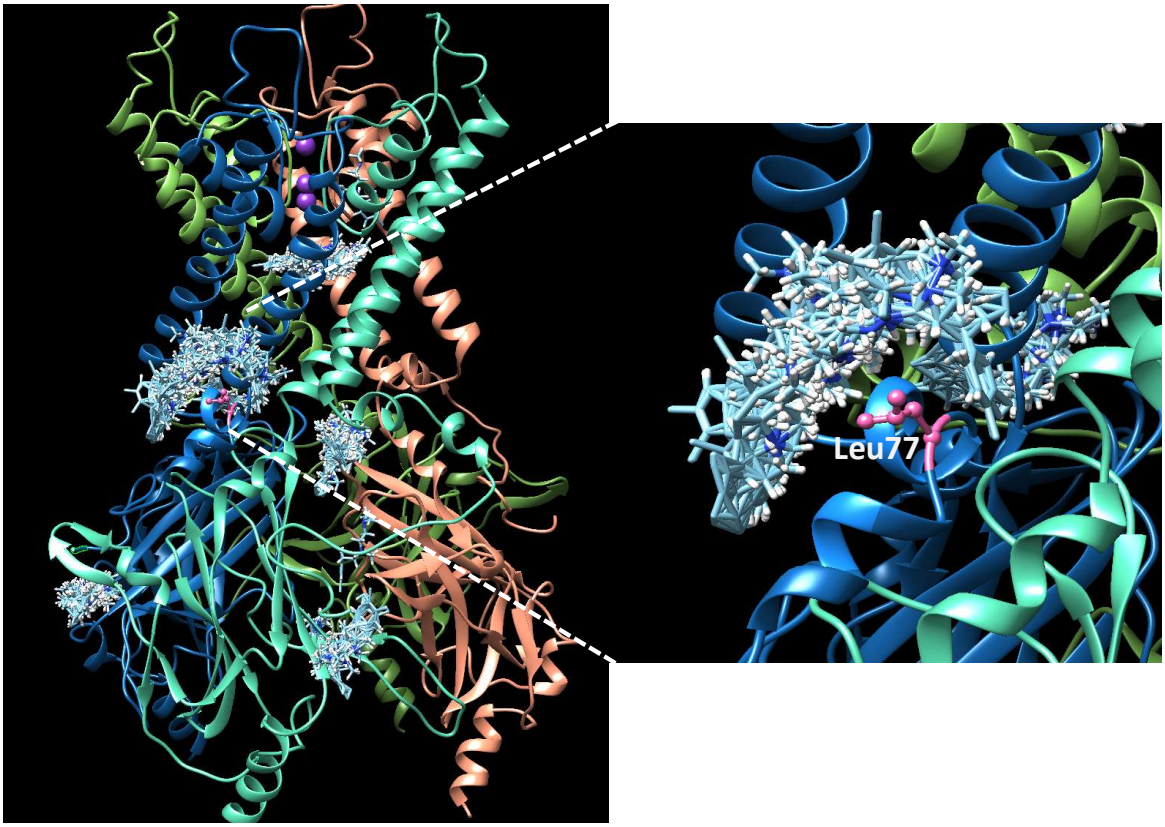

Fig. 34 Computational molecular docking of GIRK4 and BD1047 showing the contribution of Leu77

The homology structure model of GIRK4 based on the structure of GIRK2 (6XIT). Cyan clusters of BD1047 indicate the predicted dockings of BD1047 to GIRK4 in various directions and orientations. Leu77 is highlighted in pink color. A right panel is an enlarged image of Leu77 and BD1047 docking region in the left panel.

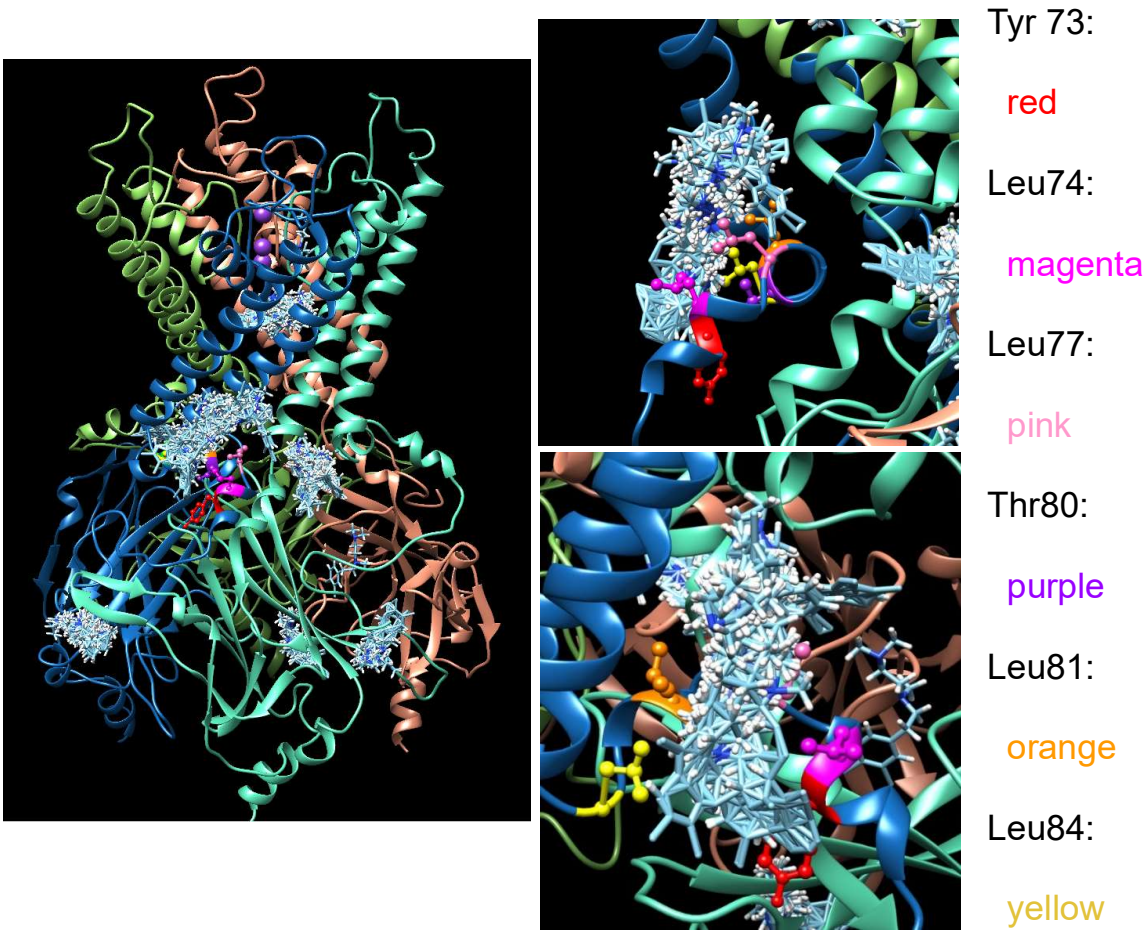

Fig. 35 Computational molecular docking of GIRK4 and BD 1047 showing contribution of amino acid residues adjacent to Leu77

The predicted protein structure is the homologous structure model of GIRK4 based on the structure of GIRK2 (6XIT). Light blue clusters of BD1047 indicate the predicted dockings in various directions and orientations of BD1047. Tyr73, Leu74, Leu77, Thr80, Leu81 and Lue84 are highlighted in red, magenta, pink, purple, orange and yellow colors, respectively. Right panel is and enlarged image of Leu77 and adjacent amino acid residues for BD interaction from the left panel.

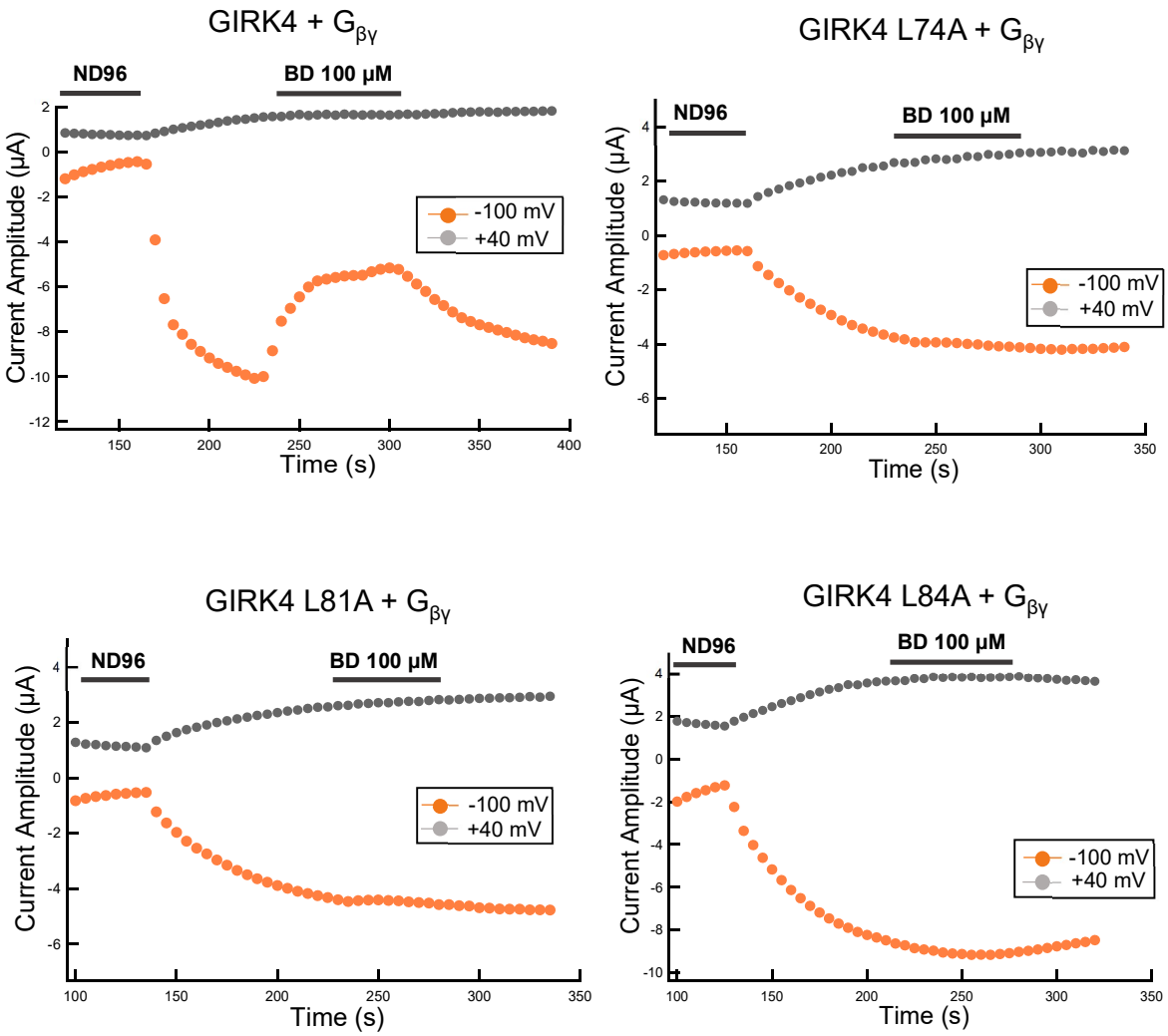

Fig. 36 The effects of BD1047 on GIRK4 and its mutants of the predicted docking sites

Time courses of current change at -100 mV (orange plots) were recorded in the absence and presence of BD1047 (100 μM) in 96K^+ solution in oocytes expressing GIRK4, GIRK4 L74A, GIRK4 L81A and GIRK4 L84A. BD1047 was applied and washed out by constant bath perfusion using a peristatic pump.

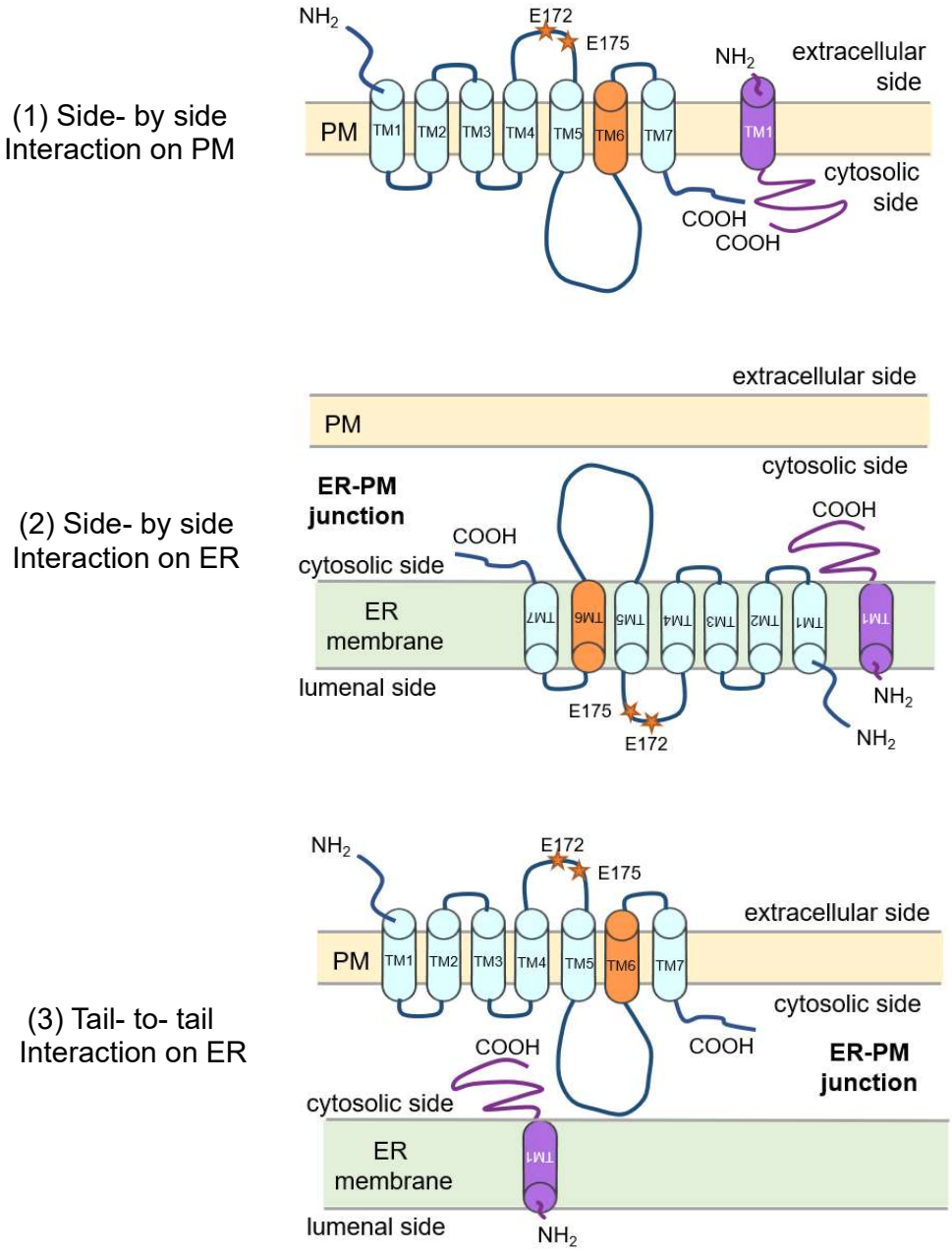

Fig. 37 Schematic drawings of the interaction manners between M2R and S1R

Side-by-side model on PM and that on ER are depicted in the upper and middle panel. Tail-to-tail model is depicted in the bottom panel. In the side-by-side model, M2R and S1R both locate on PM or on ER membrane and they interact with each other. In the tail-to-tail model, M2R locates on PM and S1R locates on ER and they interact with each other at the ER-PM junction.

Acknowledgements

It was an unexpected shift of my life from clinical medicine to the research field. I was quite lucky to meet Prof. Yoshihiro Kubo in the 5th IICC conference in China who opened the door and led me into the world of ion channels. I would like to especially thank Prof. Kubo for his inspiration, guidance and encouraging in my research. He patiently educated me basic knowledge and taught me logical thinking, presentation and writing in science. Also, thanks to him for his consideration so that I could adapt to the life in Japan as a foreign student.

I would like to thank Prof. Ruth Murrell-Lagnado (University of Sussex, Brighton, UK) who kindly shared the construct and the knowledge of S1R as well as a lot of experimental ideas for proceeding my research. And Dr. Sachiko Fujiwara (Division of Cell Structure, NIPS) who taught me the method of co-immunoprecipitation.

Here, I would like to thank former Kubo lab member, Dr. I-Shan Chen, who taught me how to do various the molecular biology experiments and how to use electrophysiological techniques as well as how to analyze the data towards reaching my experimental goals. Thanks for her kind mental support and sharing her experiences so that I could enjoy my research life in Japan.

I also would like to thank all Kubo lab members who had given me a lot discussion and suggestion in my research. Thanks to Dr. Michihiro Tateyama who taught me how to do patch-clamp and cell culture so that I could successfully conduct my experiment using mammalian cells. And thanks to Dr. Takushi Shimomura and Dr. Ki-ichi Hirazawa for their stimulating comments and encouragement for my research. Meanwhile, I would like to say thank to the former lab member, Dr. Andriani Rizki Tsari, for her kind help in my experiment and her friendship in my life. And thanks to Ms. Tomomi Yamamoto and Ms. Chizue Naito for their contribution in technical help in the lab.

Additionally, I would like to sincerely thank my best friend, Li yu, for her unconditional supports and company all the time during my PhD life. Also, many thanks to my friends, Deng yi fei, Chen xin yi, Tann, May, Long yu and Gap for bringing joys and cheering me up so that I could face the uncertainty and challenges in research and life in Japan.

Last but not the least, I would like to thank my parents and my sister for their unconditional love so that I could make this far.